



HAL
open science

Competitive effects in bacterial mRNA decay

Thibault Etienne, Muriel Cocaign-Bousquet, Delphine Ropers

► **To cite this version:**

Thibault Etienne, Muriel Cocaign-Bousquet, Delphine Ropers. Competitive effects in bacterial mRNA decay. *Journal of Theoretical Biology*, 2020, 504, 10.1016/j.jtbi.2020.110333 . hal-02967513

HAL Id: hal-02967513

<https://inria.hal.science/hal-02967513>

Submitted on 22 Aug 2022

HAL is a multi-disciplinary open access archive for the deposit and dissemination of scientific research documents, whether they are published or not. The documents may come from teaching and research institutions in France or abroad, or from public or private research centers.

L'archive ouverte pluridisciplinaire **HAL**, est destinée au dépôt et à la diffusion de documents scientifiques de niveau recherche, publiés ou non, émanant des établissements d'enseignement et de recherche français ou étrangers, des laboratoires publics ou privés.



Distributed under a Creative Commons Attribution - NonCommercial 4.0 International License

Competitive effects in bacterial mRNA decay

Thibault A. Etienne^{a,b}, Muriel Cocaign-Bousquet^a, Delphine Ropers^{b,*}

^a*TBI, Université de Toulouse, CNRS, INRA, INSA, Toulouse, France*

^b*Univ. Grenoble Alpes, Inria, 38000 Grenoble, France*

Abstract

In living organisms, the same enzyme catalyses the degradation of thousands of different mRNAs, but the possible influence of competing substrates has been largely ignored so far. We develop a simple mechanistic model of the coupled degradation of all cell mRNAs using the total quasi-steady-state approximation of the Michaelis-Menten framework. Numerical simulations of the model using carefully chosen parameters and analyses of rate sensitivity coefficients show how substrate competition alters mRNA decay. The model predictions reproduce and explain a number of experimental observations on mRNA decay following transcription arrest, such as delays before the onset of degradation, the occurrence of variable degradation profiles with increased non linearities and the negative correlation between mRNA half-life and concentration. The competition acts at different levels, through the initial concentration of cell mRNAs and by modifying the enzyme affinity for its targets. The consequence is a global slow down of mRNA decay due to enzyme titration and the amplification of its apparent affinity. Competition happens to stabilize weakly affine mRNAs and to destabilize the most affine ones. We believe that this mechanistic model is an interesting alternative to the exponential models commonly used for the determination of mRNA half-lives. It allows analysing regulatory mechanisms of mRNA degradation and its predictions are directly comparable to experimental data.

Keywords:

Michaelis-Menten kinetics, Quasi-steady-state assumption, Substrate competition, mRNA turnover, Regulation of gene expression

*Corresponding author

Preprint submitted to Journal of Theoretical Biology

May 8, 2020

1. Introduction

Intracellular levels of bacterial mRNAs result from a balance between transcription and degradation. It has long been believed that mRNA decay plays a minor role in the regulation of bacterial gene expression, most likely because bacterial transcription has been early shown the target of so many regulations. mRNA degradation has gained renewed attention when studies have evidenced tight modulations of mRNA half-life by environmental conditions, through the action of small RNAs and RNA-binding proteins (see e.g. Bobrovskyy et al., 2015; Mohanty and Kushner, 2016). Short mRNA half-lives allow both a rapid remodelling of gene expression when cells undergo environmental perturbations and a recycling of the ribonucleotide pool (Carpousis, 2007). In addition, a complicated multi-protein machinery called degradosome is responsible for both mRNA instability and RNA processing (see Marcaida et al., 2006; Lykke-Andersen et al., 2009, for reviews).

Experimental approaches for analysing mRNA decay are based on transcriptional arrest by antibiotics addition (e.g. rifampicin). The kinetics of mRNA degradation is monitored by measuring mRNA levels along time. With the advent of high-throughput technologies, this is nowadays achieved at the whole cell level using microarrays or RNA sequencing. Fitting the degradation profiles to an exponential model provides half-life values for cell mRNAs. They typically vary between 3 and 8 minutes in the model bacterium *Escherichia coli*, much shorter than the duration of the cell cycle (Bernstein et al., 2004; Chen et al., 2015; Esquerré et al., 2013). By comparison, ribosomal and transfer RNAs are stable and function over several generations. In some extreme cases in the stationary phase, half-lives as high as 50-100 minutes are measured in *E. coli* (Dressaire et al., 2018) and up to 90 minutes in the budding yeast (Wang et al., 2002).

These exponential models of mRNA decay fall short of providing mechanistic interpretations to the degradation kinetics. They are based on the assumption that mRNA decay follows a first-order reaction, that is, the reaction rate depends linearly on the mRNA concentration (Bernstein et al., 2002; Chen et al., 2015). They do not explicitly include regulations of mRNA decay, as this would require complexifying both the model and the procedure of parameter estimation. Notably, one largely ignored regulatory mechanism is the possible implication of substrate competition, while experimental studies

38 point at its possible involvement (Esquerré et al., 2015; Nouaille et al., 2017).

39

40 Substrate competition is encountered in many biochemical processes,
41 from signal transduction to gene expression or transport in living organ-
42 isms (e.g., Cookson et al., 2011; De Vos et al., 2011; Kiel and Serrano, 2012).
43 It occurs when several substrates compete for binding to the same active site
44 of an enzyme, which possibly leads to complex dynamical behaviours. For
45 instance, the substrates of the MAP kinases (MAPK), which regulate vari-
46 ous cell fate decisions (proliferation, differentiation, and apoptosis), compete
47 for binding to MAPK in early *Drosophila* embryos (Kim et al., 2010, 2011;
48 Legewie et al., 2007). Their local concentration and their relative binding
49 affinities for the MAPK is predicted to control both MAPK activity and the
50 choice of substrate. This enables the same MAPK pathway to operate in
51 different modes and elicit distinct cell type responses.

52

53 In the case of mRNA degradation, the same machinery is responsible for
54 the fate of messenger RNAs. In *E. coli* for instance, the main degradation
55 pathway is the internal cleavage of mRNAs by RNase E, an enzyme also in-
56 volved in RNA processing (Clarke et al., 2014). In the alternative, so-called
57 5'-end-dependent, pathway, mRNA cleavage by RNase E occurs after the
58 prior recognition and removal of two of the three phosphate groups at the 5'
59 end of the transcript by the pyrophosphohydrolase RppH. The fragments of
60 mRNAs are then rapidly degraded by exoribonucleases. RNase E is abun-
61 dant in *E. coli* cells (Mackie, 2013; Valgepea et al., 2013), at least in excess
62 with respect to individual substrates, but the total substrate concentration
63 largely exceeds that of the enzyme. As a consequence, pools of RNase E are
64 limited in cells. It is thus expected that differences of substrate affinities and
65 concentrations play a determinant role in the degradation kinetics of mR-
66 NAs. Experimental observations seem to agree with this hypothesis, at least
67 for mRNA initial concentrations, for which a strong negative correlation was
68 found with the mRNA lifetime (Esquerré et al., 2015; Nouaille et al., 2017).

69

70 In this manuscript, we study the possible role of substrate competition
71 on mRNA degradation kinetics. We need for this a mechanistic modelling
72 of mRNA degradation describing the binding of RNase E to competing sub-
73 strates and the subsequent titration of the enzyme. The model should make a
74 trade-off between complexity and biological realism, and have physiologically
75 interpretable parameters. In addition model predictions should be directly

76 comparable to experimental data. Common models of mRNA degradation ki-
77 netics do not meet this requirement. We thus developed a mechanistic model
78 of mRNA decay in this study and analysed the effect of mRNA competition
79 on the degradation kinetics.

80 In what follows, we briefly survey mRNA degradation (Section 2). We
81 show in Section 3 how to assimilate mRNA degradation by the degrado-
82 some to a macro-reaction catalysed by the limiting enzyme RNase E. The
83 kinetics of the reaction is described by means of a Michaelis-Menten equa-
84 tion. To take into account the fact that RNase E is in limited concentration
85 with respect to all mRNA concentrations, we used the tQSSA form of the
86 Michaelis-Menten equation for describing the degradation kinetics. By ex-
87 tending previous works by Pedersen et al. (2007) and Tang and Riley (2013),
88 we developed an approximated version of the tQSSA form which includes
89 competition between all cell mRNAs. We used this approximation in Sec-
90 tion 4 to study the contribution of competition to mRNA decay by means
91 of numerical simulations, based on carefully chosen parameter values and
92 distributions. Our results show that the introduction of competition leads
93 to variability, delays and increased non linearities in the degradation curves,
94 similarly to experimental observations. Such diversity and non linearities are
95 difficult if not impossible to reproduce in the absence of competition. By
96 means of rate response coefficients in Section 5 and 6, we show how competi-
97 tion globally affects degradation by slowing it down and how it differentially
98 affects the fate of mRNAs. We discuss these results in Section 7.

99 **2. A short survey of mRNA degradation: mechanism, monitoring** 100 **and kinetic modelling**

101 *2.1. The mechanism of mRNA degradation and its regulation*

102 In many bacteria, RNase E (EC 3.1.26.12) is a central player of mRNA
103 degradation and RNA processing. It initiates the processing of small RNAs
104 and of a majority of pre-tRNAs, participates to the maturation of riboso-
105 mal RNAs in addition to degrading mRNAs. The tetrameric enzyme forms
106 a multi-protein complex called the RNA degradosome, together with the
107 RNA helicase B (RhlB), the glycolytic enzyme enolase (Eno), and the phos-
108 phorolytic exonuclease polynucleotide phosphorylase (PNPase) (Carpousis,
109 2007). It is mostly anchored to the cytoplasmic inner membrane, where it
110 forms highly mobile foci diffusing all over the membrane (Strahl et al., 2015).

111 These foci disappear upon inhibition of transcription and the subsequent dis-
112 appearance of mRNAs.

113

114 mRNA degradation results from the combined action of endo- and exo-
115 ribonucleases (Fig. 1). As an endoribonuclease, RNase E catalyses the first
116 internal cleavage, followed by a rapid degradation of the RNA fragments by
117 exoribonucleases. This initial cleavage is considered to be the limiting step in
118 mRNA degradation (Kushner, 2002). RNase E has also an indirect effect on
119 mRNA decay, through the processing of small regulatory RNAs that regulate
120 the stability of their target mRNAs (Chao et al., 2017). This is for instance
121 the case of CsrB and C, which control the activity of the post-transcriptional
122 regulator CsrA. Their stabilization or destabilization alters the half-life of
123 many CsrA-regulated genes (Suzuki et al., 2006).

124

125 The gene coding RNase E is essential, presumably due to its role in RNA
126 processing. Knocking down RNase E activity *in vivo* or decreasing its cel-
127 lular level result in a slowdown in the turnover of bulk mRNAs (Bernstein
128 et al., 2004; Sousa et al., 2001; Stead et al., 2010). Microarray analyses have
129 shown RNase E to initiate the decay of 60% of *E. coli* mRNAs (Bernstein
130 et al., 2004; Stead et al., 2010). Recently RNA-seq experiments have mapped
131 thousands of RNase E cleavage sites in both *E. coli* and *Salmonella* tran-
132 scriptomes (Chao et al., 2017; Clarke et al., 2014). Other endoribonucleases
133 have been identified, such as RNase III and the paralog of RNase E in *E. coli*,
134 RNase G, but they have a much more limited set of substrates (Carpousis,
135 2007; Kushner, 2002).

136

137 RNase E prefers binding to single-stranded RNA regions that are typically
138 A-U rich, with a strong preference for U at position +2 with respect to the
139 scissile phosphate (Chao et al., 2017; Clarke et al., 2014; Huang et al., 1998;
140 McDowall et al., 1994, 1995). Two determinants of substrate recognition
141 are the 5'-monophosphate termini – known to activate degradation through
142 a higher enzyme affinity (Kime et al., 2010; Mackie, 1998) – and the pres-
143 ence of a stem-loop upstream of the cleavage site in most mRNAs cleaved by
144 RNase E (Del Campo et al., 2015). The current model proposes two modes of
145 substrate recognition, which do not need to be mutually exclusive (Bandyra
146 et al., 2018). In the 5'-sensing mode, RNase E binds to the 5' monophos-
147 phate and the first bases of the 5' termini, causing an appropriate alignment
148 at the active site of the single-stranded region containing the cleavage site.

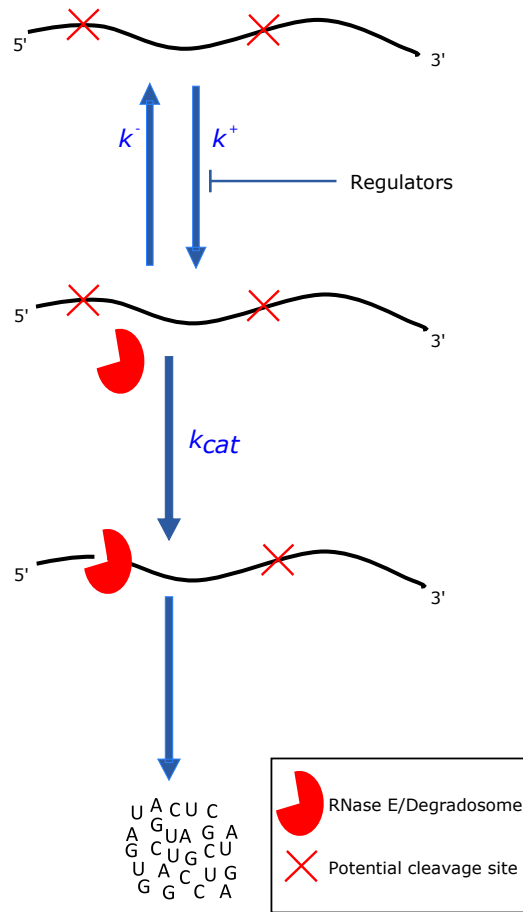


Figure 1: RNA degradation in Prokaryotes. Endoribonucleolytic cleavage by RNase E generates fragments that are further converted to nucleotides by oligoribonucleases. RNase E binds to a A-U rich sequence of the messenger RNA, often downstream of a stem loop. The binding can be strengthened or weakened by regulatory proteins or RNAs. k^+ and k^- are the rate constants for the association and dissociation of RNase E to the mRNA, respectively. k_{cat} is the catalytic constant of the degradation reaction.

149 In this case, degradation by RNase E requires a preliminary processing by
 150 RppH of the 5'-triphosphate termini to 5'-monophosphate (Celesnik et al.,
 151 2007; Deana et al., 2008; Garrey and Mackie, 2011). In the 5' bypass mode,
 152 which seems to be the most frequent one (Clarke et al., 2014; Richards et al.,
 153 2012), the direct binding of RNase E to a structured region of the mRNA
 154 allows to align the single-strand region at the active site independently of
 155 the nature of the 5' end (Bandyra et al., 2018).

156

157 The binding of RNase E to individual bacterial mRNAs is also regulated
158 by trans-acting factors (Fig. 1) (Richards and Belasco, 2019). The base pair-
159 ing of a small RNA with a mRNA can lead for instance to translational
160 activation or repression in response to stresses. The later case is often asso-
161 ciated to an increased destabilization of the messenger RNA. In many cases
162 the process involves the protein chaperone Hfq, which facilitates the base
163 pairing between the sRNA and the mRNA (see for review Santiago-Frangos
164 and Woodson, 2018). Ribosomes bound to the ribosome-binding site protect
165 mRNAs from degradation by RNase E (for review, Deana and Belasco, 2005).
166 Changes in the level and activity of RNase E also modulates the degradation
167 rate. An auto-regulation mechanism has been shown sensing the intracellular
168 level of RNase E (Jain and Belasco, 1995a). However, under normal circum-
169 stances there appears to be excess RNase E in the cell, because enzyme levels
170 have to be significantly reduced to see any phenotypic effect (Jain and Be-
171 lasco, 1995b). The regulatory proteins RraA and RraB were also shown to
172 repress RNase E activity *in vivo* when over-expressed (Lee et al., 2003), but
173 their physiological role remains to be determined.

174 2.2. Monitoring mRNA degradation kinetics

175 Current experimental methods monitor mRNA decay in Prokaryotes and
176 Eukaryotes through three different approaches: general inhibition of tran-
177 scription by drugs (e.g. rifampycin) or mutation, transcriptional control
178 by regulatable promoters and pulse-chase labelling (Lugowski et al., 2018).
179 Transcription is inhibited in the two first cases, either that of all cellular
180 genes or of a single gene, following which the mRNA level starts to decay.
181 Pulse-chase labelling relies on the cell incorporation of labelled nucleotides
182 into newly synthesized RNAs. The addition of natural nucleotides wash out
183 the labelled nucleotides. mRNA decay is then monitored by following the
184 decline of labelled mRNAs.

185

186 Transcription inhibition is often used in Prokaryotes (see Bernstein et al.,
187 2002; Esquerré et al., 2014; Dressaire et al., 2018; Hundt et al., 2007, for
188 a few examples), coupled nowadays to high throughput technologies for the
189 quantification over time of residual mRNA concentrations. Large scale data
190 obtained with micro-arrays are by far the most abundant in the literature
191 (for review Laguerre et al., 2018). At the time of transcription inhibition and

192 in the following minutes, the culture is sampled, mRNAs are extracted, pu-
193 rified, and used as matrix for the synthesis of complementary cDNAs. The
194 latter are then quantified by hybridization to DNA chips. As an illustra-
195 tion, mRNA degradation profiles obtained in *E. coli* with this approach are
196 shown in Appendix A.1. Alternatively, qRT-PCR approaches allow obtain-
197 ing medium scale data through the amplification of selected cDNAs. RNA
198 sequencing approaches starts also being used (Chen et al., 2015; Laguerre
199 et al., 2018; Moffitt et al., 2016; Potts et al., 2017). They consist in the
200 depletion of ribosomal RNAs and the retro-transcription of mRNAs into cD-
201 NAs, before the latter are sequenced.

202

203 Depending on the method chosen for the quantification of residual mR-
204 NAs, different types of data normalization can be applied (Laguerre et al.,
205 2018). The objective is to compensate for technical variations between sam-
206 ples at different time points. The mRNA levels can be further multiplied
207 by RNA extraction yields to obtain mRNA concentrations in arbitrary units
208 per gram dry weight. Mathematical models are subsequently used to esti-
209 mate mRNA half-lives from these normalized data, as we shall see in the
210 following section. Other modelling efforts include mRNA degradation beside
211 other processes, some models being used to analyse regulatory mechanisms
212 of mRNA degradation kinetics.

213 2.3. Kinetic modelling of mRNA degradation in literature

214 Various mathematical models of mRNA degradation kinetics have been
215 proposed in the literature, the most common and simplest one being the
216 exponential model. This mathematical description simplifies the mechanism
217 of mRNA degradation to a first-order reaction modelled by the following
218 linear ordinary differential equation (ODE):

$$\frac{d}{dt}m_i(t) = -k_{deg_i}m_i(t), \quad m_i(0) = m_{i0} \quad (1)$$

219

220 where $m_i(t)$ is the concentration at time t of the messenger RNA of gene i .
221 k_{deg} is the degradation constant, from which mRNA half-life can be determined:
222 $t_{1/2} = \log(2)/k_{deg}$. This model is valid once transcription has been stopped at
223 time 0, which means that the transcription rate does no longer counterbalance the
224 degradation rate of mRNAs.

225

226 This mathematical modelling implies that the degradation kinetics depends lin-
227 early on the initial concentration of mRNA i , according to the following analytical
228 solution of the ODE system:

$$m_i(t) = m_{i0} \times e^{(-k_{deg_i} \times t)}. \quad (2)$$

229
230 The exponential model in Eq. 2 is commonly used to estimate mRNA half-life
231 by linear regression on a semilog plot of the concentration levels (for review, La-
232 guerre et al 2018). The approach has been used for decades to estimate individual
233 mRNA half-lives. It has been extended more recently to genome-wide data (e.g.
234 Bernstein et al., 2002, 2004; Esquerré et al., 2014; Potts et al., 2017). Other related
235 models are now emerging. They extend the exponential model with a delay before
236 the onset of the decay (Chen et al., 2015; Dar and Sorek, 2018; Moffitt et al.,
237 2016) and a residual mRNA concentration at the end of the degradation process
238 (Moffitt et al., 2016). The delay is generally attributed to the time required by
239 RNA polymerase to complete transcription initiated prior to the drug addition.

240
241 First-order models provide valuable information on reaction rates through the
242 determination of mRNA half-lives. However, they fell short of describing the
243 biological mechanisms at work. In the literature, mechanistic models including
244 mRNA degradation are generally broader in scope. With a relative simple de-
245 scription of the degradation mechanism, they relate several cellular processes such
246 as the synthesis and degradation of mRNAs and proteins, the DNA replication and
247 the cell growth... (e.g. Tadmor and Tlusty, 2008; Thomas et al., 2018; Weiße et al.,
248 2015). In (Thomas et al., 2018) for instance, mRNA degradation is identified as
249 one source of growth heterogeneity at slow grow rates, when ribosomes are in too
250 low numbers to protect mRNA from degradation by endonucleases. This leads to
251 variations in biomass production and division times. Some modelling efforts are
252 more focused on the mechanism of mRNA degradation and its regulation, such as
253 the 5' binding and sliding of endonucleases on mRNAs and the mRNA protection
254 by ribosomes in bacteria (Carrier and Keasling, 1997; Deneke et al., 2013), or else
255 the modes of action of miRNAs on protein translation and mRNA degradation in
256 Eukaryotes (Morozova et al., 2012). For instance, Carrier and Keasling (1997) and
257 Deneke et al. (2013) have developed models of this type using a stochastic frame-
258 work. However, the simulation of these models comes with a computational cost,
259 which makes it inappropriate to analyse the coupled degradation of all cell mRNAs.

260
261 Knowing that large scale data are mostly available for mRNA degradation
262 nowadays, these mechanistic modelling studies tell us that a compromise has to
263 be reached in terms of model complexity and biological realism. The ideal model

264 should i) be realistic from a biological point of view and useful to analyse regu-
265 latory mechanisms of mRNA degradation including competition; ii) alleviate the
266 computational cost of numerical simulations; iii) include parameters that can be
267 interpreted from a biological point of view; and iv) predict degradation kinetics
268 that can be directly confronted to experimental data. We develop in the follow-
269 ing section a kinetic model of the coupled degradation of all cell mRNAs, which
270 meets these constraints as much as possible. We justify how we simplified the
271 complexity of mRNA degradation to a macro-reaction catalysed by the limiting
272 enzyme RNase E. We modelled this reaction and its regulations with the total
273 quasi-steady-state approximation of the Michaelis-Menten equation. We incor-
274 porate substrate competition among the regulatory mechanisms. This required
275 extending earlier modelling works on substrate competition to the case when mul-
276 tiple substrates compete for the same enzyme and when individual substrates are
277 in excess of enzyme, but not the total substrate concentration.

278 **3. Model development**

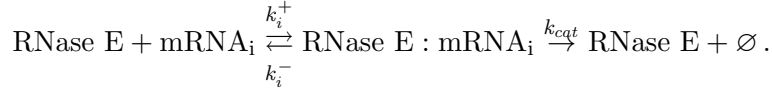
279 *3.1. Simplified description of mRNA degradation*

280 As explained in Section 2.3, developing a model that can be confronted to
281 experimental data constrains the level of description and the nature of the mecha-
282 nisms to consider. We described in Section 2.2 how high throughput approaches are
283 used to quantify residual mRNA concentrations after transcriptional arrest. These
284 approaches quantify full length mRNAs through a good coverage of mRNA se-
285 quences. For instance, qRT-PCR and microarray experiments make use of oligonu-
286 cleotides distributed along mRNAs (see Esquerré et al., 2014; Nouaille et al., 2017,
287 for example), and read counts for each gene are determined in RNAseq experi-
288 ments. In other words, messenger RNAs that have been cut once or several times
289 by endo- and exo-nucleases are not tractable in these experiments. Especially
290 since the rapidity of degradation by exonucleases makes it unlikely that partially
291 degraded mRNAs could be confused with full length mRNAs. According to Fig. 1,
292 this implies that our model does not need to describe reaction steps posterior to
293 the initial cleavage by the endoribonuclease. In most cases, the endoribonuclease
294 is RNase E and we will refer to that enzyme hereafter, although in some cases
295 other endoribonucleases like RNase G are known to specifically degrade some tar-
296 get mRNAs. Our model remains valid for these alternative enzymes as well.

297

Experiments monitor the disappearance of full length mRNAs following the
binding of RNase E to these mRNAs and their internal cleavage. As summarized in
Section 2.1, this is the limiting step in mRNA degradation. The initial cleavage by
RNase E is followed by the complete degradation of mRNAs into ribonucleotides,

which implies that the reaction is irreversible and we do not expect end-product inhibition. So essentially, the simplest mechanistic description of mRNA degradation would simplify the reaction steps in Fig. 1 to the binding of free RNase E to a given mRNA i and its subsequent cleavage according to the general biochemical equation:



298

299 The rate constants k_i^+ and k_i^- denote respectively the rate of association or
 300 dissociation of mRNA $_i$ with the enzyme. Sequence and structure specificities may
 301 affect the rate at which RNase E binds to or unbinds from mRNAs. k_{cat} is the
 302 catalytic constant of the reaction. The nature of the 5' extremity of some mRNAs
 303 is known to affect this constant when the 5' sensing mode is the mechanism of sub-
 304 strate recognition. In this case, RNase E can bind to mRNAs with 5' triphosphate
 305 termini but do not cleave them due to steric hindrance (Mackie, 1998; Callaghan
 306 et al., 2005). These mRNAs need a pre-processing by RppH to convert the 5'
 307 triphosphate into a 5' monophosphate termini. The conversion of the 5' end by
 308 RppH seems to concern only a small fraction of each transcript (Luciano et al.,
 309 2017; Richards et al., 2012), but the fact has not been established for all cell mR-
 310 NAs. Given that the direct entry mechanism is the most frequently used and that
 311 it functions independently of the 5' end, we will thus consider for simplicity that
 312 the catalytic constant is the same for all mRNAs. According to this view, the
 313 recognition of the 5' end is expected to act on the enzyme affinity only, in agree-
 314 ment with Kime et al. (2010).

315

316 The binding of RNase E to its target mRNA can be modulated, for instance
 317 by small RNAs, regulatory factors such as the proteins Hfq and CsrA, trans-
 318 lating ribosomes or else, as we shall see later, by competition between mRNAs.
 319 In the following section, we will show how to model the biochemical equation
 320 and its regulation. This equation is reminiscent of enzymatic reactions driven
 321 by Michaelis-Menten kinetics. However, we will see that the classical Michaelis-
 322 Menten expression based on the standard quasi-steady-state approximation does
 323 not always hold for this particular system along the degradation kinetics and for
 324 all mRNAs.

325 3.2. Kinetic modelling using quasi-steady-state approximations

326 Measurements of residual mRNA concentrations are performed experimentally
 327 on populations of sampled cells. We will thus use a deterministic modelling frame-
 328 work to describe the degradation kinetics. The model will predict averaged in-

329 tracellular mRNA concentrations over the population of cells that can be related
330 directly to experimental data.

331 In biochemistry, Michaelis-Menten-Henri kinetics is classically used to model
332 enzymatic reactions (for review, Cornish-Bowden, 2013). The expression is de-
333 rived from mass-action law and additional simplifying hypotheses introduced by
334 Briggs and Haldane (1925), based on a standard quasi-steady-state approximation
335 (sQSSA). It relates the reaction rate to the substrate concentration. This gives
336 the following formula with our system:

$$v_i = -\frac{d}{dt}m_i(t) = \frac{Vm \times m_i(t)}{Km_i + m_i(t)}, \quad (3)$$

337 where $m_i(t)$ is the total concentration of mRNA i , assumed to be equal to the
338 free substrate concentration: $m_i(t) \simeq m_{i,free}(t)$. $Vm = k_{cat}E_0$ is the maxi-
339 mum velocity achieved by the system at saturating concentration of mRNA i
340 and E_0 is the total enzyme concentration. The value of the Michaelis constant
341 $Km_i = (k_{cat} + k_i^-)/k_i^+$ is defined as the substrate concentration at half maximum
342 velocity. Kinetic parameters and concentrations are in standard units: molar units
343 for Km values and intracellular concentrations, and min^{-1} for the k_{cat} .

344

345 The sQSSA form of Michaelis-Menten kinetics in Eq. 3 reduces not only the
346 model complexity but also allows relating model predictions with experimental
347 observations. This canonical equation is commonly used in biochemical models,
348 without regard to the validity of the underlying assumptions. Under the sQSSA,
349 however, the substrate concentration must be greater than the enzyme concentra-
350 tion and the following relation should hold in our conditions: $Km_i + m_i^T \gg E_0$,
351 where m_i^T is the total concentration of mRNA i corresponding to the concen-
352 trations of the free form of mRNA i , its form complexed to RNase E and the
353 degradation product. This condition is verified in most *in vitro* enzymatic assays,
354 where the enzyme concentration is chosen much lower than the substrate concen-
355 tration.

356

357 However, the sQSSA condition can break down in *in vivo* conditions (e.g. Albe
358 et al., 1990; Sols and Marco, 1970). Intra-cellular enzyme concentrations are usu-
359 ally higher or at least of the same magnitude as their substrates. Consequently, a
360 significant fraction of substrates can be bound as complexes (Bennett et al., 2009).
361 What happens to mRNA degradation? The difficulty to verify sQSSA validity lies
362 in the fact that Km_i values are unknown. Available values in the literature were
363 obtained in *in vitro* assays using synthetic RNAs and resulted in variable values
364 whose validity in *in vivo* conditions is questionable (Jeske et al., 2018; Jiang and
365 Belasco, 2004; Kim et al., 2004; Kime et al., 2008, 2010). We expect that Km

366 values *in vivo* vary between mRNAs due to sequence and structure specificities.
 367 Regulations by small RNAs or RNA-binding proteins may affect as well the affinity
 368 of the enzyme for its substrates. Quantitative data are available for the concen-
 369 trations of RNase E and mRNAs though. For example, Valgepea et al. (2013)
 370 have quantified these concentrations in *E. coli* cultures growing at various rates
 371 in steady state. It appears that the median mRNA concentration at $0.48h^{-1}$ (0.5
 372 nM) is way smaller than the concentration of the tetrameric form of RNase E (411
 373 nM). This enzyme excess with respect to individual mRNAs is no longer observed
 374 at the mRNA population level, since the total concentration of mRNAs is much
 375 larger (5927 nM).

376
 377 An alternative to sQSSA is the total quasi-steady-state approximation (tQSSA)
 378 (Borghans et al., 1996; Tzafirri, 2003). It replaces the concentration of free sub-
 379 strate with its total concentration. Unmistakably, the total substrate cannot be
 380 depleted by the formation of a complex with the enzyme. As a consequence of
 381 this simple modification, tQSSA is valid for almost any substrate and enzyme con-
 382 centrations. Its domain of validity is also larger than a third approximation, the
 383 reverse quasi-steady state approximation (rQSSA), which assumes that the sub-
 384 strate concentration is in quasi-steady-state with respect to that of the enzyme-
 385 substrate complex (Schnell and Maini, 2000; Segel and Slemrod, 1989; Tzafirri and
 386 Edelman, 2004). The rQSSA is valid for high enzyme concentrations and would
 387 be appropriate to describe the degradation of individual mRNAs but not for a
 388 population of mRNAs. For these reasons of larger domain of validity, we will thus
 389 use the total QSSA of the Michaelis-Menten equation. Moreover, this in line with
 390 the experimental procedure, which most likely quantifies the total pool of mRNAs
 391 due to their deproteination following cell lysis. In the next section, we describe
 392 the modelling of the degradation of individual mRNAs using total QSSA. We will
 393 extend further the model in Section 3.4 with mRNA competition.

394 3.3. Kinetic modelling of the enzymatic degradation of individual mRNAs

395 We start here with the simplest case of mRNA degradation, where mRNAs are
 396 isolated and do not compete for binding to RNase E. This allows us to develop
 397 a simple model for the degradation of isolated mRNAs, which we will refer to as
 398 'isolated system' in the rest of the article. We denote $m_{i,free}(t)$ the free concen-
 399 tration of mRNA i . $c_i(t)$ is the concentration of complex *RNase E : mRNA_i*. We
 400 have the following mass conservation relation for the total concentration of mRNA
 401 i :

$$m_i(t) = m_{i,free}(t) + c_i(t). \quad (4)$$

402

403 Employing the total substrate concentration instead of the free concentration
 404 results in the so-called single reaction tQSSA (Borghans et al., 1996; Tzafiriri,
 405 2003). This equation is virtually valid for any substrate and enzyme concentra-
 406 tions:

$$\frac{d}{dt}m_i(t) = \frac{-k_{cat} \times \frac{E_0 + Km_i + m_i(t)}{2}}{-\frac{\sqrt{(E_0 + Km_i + m_i(t))^2 - 4 \times E_0 \times m_i(t)}}{2}}, \quad m_i(0) = m_{i0}. \quad (5)$$

407

408 From the somewhat complex expression in (5), Tzafiriri (2003) developed an
 409 approximation called first order tQSSA. It resembles the sQSSA form of Michaelis-
 410 Menten kinetics:

$$\frac{d}{dt}m_i(t) = -\frac{k_{cat} \times E_0 \times m_i(t)}{Km_i + E_0 + m_i(t)} \quad (6)$$

411

412 The equation (6) is valid if either of the following criteria is satisfied. Let K_i
 413 be the individual constant of Van Slyke defined by $K_i = k_{cat}/k_i^+$:

$$E_0 + Km_i \gg m_{i0} \quad \text{and} \quad K_i \ll Km_i \quad \text{or} : \quad (7)$$

$$E_0 \gg m_{i0} \quad \text{and} \quad E_0 \gg Km_i \approx K_i \quad (8)$$

414

415 As for the sQSSA form of the Michaelis-Menten, model parameters are ex-
 416 pressed in the same international standard units. Note that the comparison of
 417 model predictions generated by these models with experimental data may require
 418 preliminary conversions or normalizations. Indeed, some experimental protocols
 419 used for mRNA quantification generate data in arbitrary units. For instance, mi-
 420 croarrays quantifying residual mRNAs generate concentrations in arbitrary units
 421 per gram dry weight (see Esquerré et al., 2013, for instance), and Ct values for
 422 qRT-PCR data (e.g. Nouaille et al., 2017).

423 3.4. Model extension with competition between mRNAs

424 The tQSSA derived in the previous section is well adapted for the description
425 of the degradation of isolated mRNAs. However, the reality is that cells include a
426 large number of mRNAs that share the same degradation enzyme, not to mention
427 the small RNAs, pre-tRNAs and pre-rRNAs that are also processed by RNase E.
428 Can these multiple substrates titrate the enzyme?

429 To the best of our knowledge, there is no direct experimental evidence for com-
430 petition, through measurements of the intracellular concentration of free or bound
431 RNase E for instance. However, several studies support indirectly this hypothesis.
432 *E. coli* cells transcribe mRNAs from about 4000 genes, resulting in a much higher
433 intracellular mRNA concentration with respect to the enzyme (Section 3.1). Their
434 capacity to titrate RNase E depends on the enzyme kinetic properties. An efficient
435 enzyme would process the excess of mRNA without being significantly titrated.
436 However, available data for RNase E suggest that the enzyme is far from being
437 a kinetically perfect enzyme (see Table B.1 for details). The rate of turnover of
438 the mRNA-RNase E complex is rather small (11 min^{-1} on average), while the
439 low K_m value ($0.4 \mu\text{M}$) indicates a rapid binding of mRNAs to the enzyme. This
440 suggests that the enzyme cannot process the excess of mRNA efficiently and that
441 significant enzyme titration can be expected. A similar regulatory mechanism has
442 been proposed for another ribonuclease with a much smaller set of substrates in
443 *E. coli*, RNase P. This enzyme is involved in the maturation of the 5' end of eighty
444 tRNA precursors (Yandek et al., 2013).

445 Among the multiple RNase E substrates, those at higher concentration have
446 generally a better chance to bind to the poorly available enzyme and be degraded.
447 This has been experimentally observed by means of reporter genes in *E. coli*
448 (Nouaille et al., 2017). Increasing the concentration of given mRNAs reduced their
449 stability, which is an indirect evidence supporting the existence of competition in
450 RNase E-mediated degradation.

451 Along these lines, mRNAs would thus compete for binding to the active site
452 of RNase E (Fig. 2), with the consequence that the rate of formation and the
453 concentration of the complex between a mRNA i and RNase E might influence
454 other mRNAs j . We thus extend the model in Section 3.3 to include competition
455 between mRNAs. We will refer to this system as 'competitive' in the rest of the
456 paper.

457

458 The competition between mRNAs requires to track the free enzyme concen-
459 tration. This was done in (Pedersen et al., 2007), in which the authors studied the
460 case of two competing substrates. Tang and Riley (2013) extended this work to

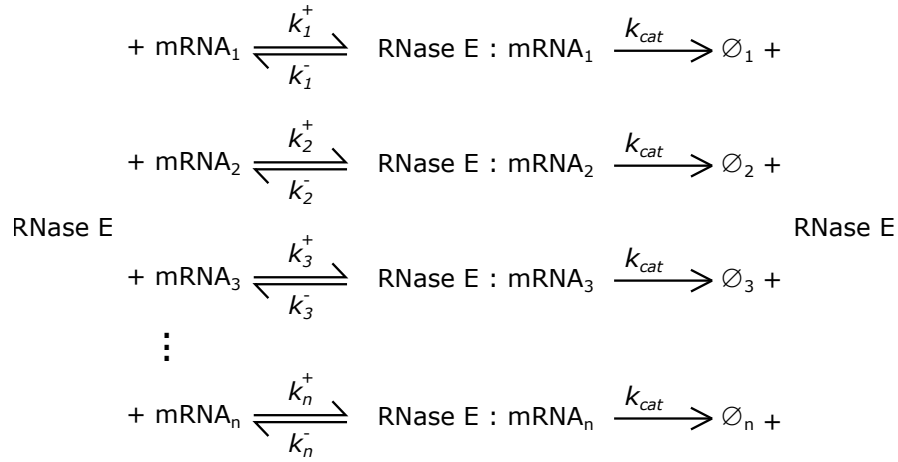


Figure 2: mRNA degradation by RNase E in conditions of limiting enzyme concentration. \emptyset_i denotes the degradation product of mRNA i .

461 complex systems with n substrates, m enzymes and different types of inhibitory
462 mechanisms. The authors also studied the special case of a system with n sub-
463 strates and one enzyme (Eq. 20 in Tang and Riley (2013)). We applied this deriva-
464 tion to the case of n mRNAs competing for binding to RNase E. Using mass-action
465 law, we wrote the following ODE system, with $i = 1, \dots, n$ mRNAs (see Appendix
466 C for details):

$$\begin{aligned}
\frac{d}{dt} m_i(t) &= -k_{cat} \times c_i(t), \quad m_i(0) = m_{i0} \\
\frac{d}{dt} c_i(t) &= k_i^+ \times [(E_0 - \sum_{j=1}^n c_j(t)) \\
&\quad \times (m_i(t) - c_i(t)) - K m_i \times c_i(t)], \quad c_i(0) = 0.
\end{aligned} \tag{9}$$

467
468 In their respective works, Pedersen et al. (2007) and Tang and Riley (2013) ap-
469 plied approximations to the mass-action law system. They used the quasi-steady-
470 state approximation $\frac{dc_i(t)}{dt} \sim 0$ and either the total two Padé approximation (Ped-
471 ersen et al., 2007) or perturbation theory (Tang and Riley, 2013) to eventually
472 obtain similar expressions. The application of the global approximation in (Tang
473 and Riley, 2013) to our system of competition allowed us to obtain a simplified
474 formula, much easier to interpret, which can be related to other Michaelis-Menten
475 expressions (see Appendix C for details):

$$\frac{d}{dt}m_i(t) = -\frac{k_{cat} \times E_0 \times m_i(t)}{Km_i \times \left(1 + \sum_{j \neq i} \frac{m_j(t)}{Km_j}\right) + E_0 + m_i(t)} \quad (10)$$

476

477 with $j = 1 \dots n$.

478

The expression differs from the model of the isolated system in Eq. 6 with the introduction of a competition term $(1 + \sum_{j \neq i} (m_j(t)/Km_j))$ multiplied to the Km value, similarly to competitive inhibition systems. We will refer to the resulting constant

$$Km_i^{app}(t) = Km_i \times \left(1 + \sum_{j \neq i} \frac{m_j(t)}{Km_j}\right)$$

479

as "apparent Km" in the rest of the article. The competition term increases the value of the apparent Km value, indicative of a reduced RNase E affinity for its target mRNAs in competitive systems compared to isolated systems.

482

483

Tang and Riley (2013) studied the range of enzyme and substrate concentrations for which their approximation is valid. Pedersen et al. (2007) give also these criteria of validity, as well as the range of Km values for the system with two competing substrates. We could easily extend these criteria to the case of a system with multiple competing substrates. With $K = \frac{k_{cat}}{\min\{k_{1,i}\}}$, any of the following conditions imply the validity of the approximation:

485

486

487

488

$$\begin{aligned} E_0 \ll Km_i^{app}(0) + m_{i0} \quad \text{and} \quad K \lesssim Km_i^{app}(0) + m_{i0} \\ Km_i \gg \sum_{i=1}^n m_{i0} \quad \text{and} \quad K \ll Km_i^{app}(0) \\ Km_i \gg \sum_{i=1}^n m_{i0} \quad \text{and} \quad E_0 \gg K \gtrsim Km_i^{app}(0) \\ E_0 \gg Km_i^{app}(0) + m_{i0} \quad \text{and} \quad E_0 \gg K \end{aligned}$$

489

490

491

Using numerical simulations of *in vivo* reactions, Pedersen et al. (2007) showed that their approximation is valid for a large range of parameter values. It fits

492 correctly the original mass-action law model. In (Tang and Riley, 2013), the gen-
493 eralisation of the approximation to multiple substrates and/or enzymes prove to
494 outperform the Michaelis-Menten expression. We will use in what follows this
495 approximated version to investigate competitive effects in mRNA degradation ki-
496 netics.

497 **4. Numerical simulation of mRNA degradation kinetics in isolated** 498 **and competitive systems**

499 At this stage, we have developed two alternative models of mRNA degrada-
500 tion kinetics in bacteria. Both rely on approximations of tQSSA forms of the
501 Michaelis-Menten expression with extended criteria of validity compared to the
502 classical sQSSA form. One model describes the reaction kinetics in situations
503 where mRNAs are isolated and degraded independently of other mRNAs (Eq. 6).
504 The second model includes the effect of competition between substrates, where
505 the formation of complexes between RNase E and mRNAs possibly affects the
506 formation of other complexes (Eq. 10). Whether this is a true phenomenon in the
507 control of mRNA turnover or not has not been established. Two recent studies
508 suggest that this might be the case, since mRNAs with higher concentrations are
509 destabilized in the bacteria *E. coli* and *Lactococcus lactis* (Esquerré et al., 2015;
510 Nouaille et al., 2017). It has been proposed that higher mRNA concentrations
511 increase the probability that RNase E encounters its substrates in these two bac-
512 terial strains.

513

514 Although our two models are relatively simple at first glance, the introduction
515 of competition between mRNAs couples the ordinary differential equations. This
516 makes the system behaviour difficult to understand intuitively, in particular when
517 studying degradation of all cell mRNAs. We will rather rely on numerical simula-
518 tions for our purpose. This requires setting parameters to reasonable physiological
519 values in order to predict degradation kinetics. Since literature data on the subject
520 are generally scarce, we will use data obtained in the bacterium *E. coli* for which
521 more knowledge and quantitative information are available. However, the model
522 structure is sufficiently general and the mechanisms considered, well conserved
523 among bacteria, for the model to be valid in other biological backgrounds.

524 *4.1. Model parameters and initial conditions*

525 Our objective with the models is to generate progress curves comparable to
526 those obtained experimentally. The experimental curves vary a lot, from expo-
527 nential to more linear shapes (see Appendix A.1 as an example). Their fitting by
528 an exponential function allows determining mRNA half-lives ranging from one up

529 to a dozen of minutes. This variability in mRNA stability reflects the diversity
530 of mRNA sequence and structure determinants that modulate the enzyme affinity
531 for its targets. It also results from regulatory mechanisms, such as regulations by
532 small RNAs or mRNA protection by ribosomes to name but a few, which also im-
533 pact the binding of RNase E to mRNAs. According to our modelling hypotheses
534 described in Section 3.1, this results in an expected large variability of Km values
535 because the k_{cat} value is held constant between mRNAs.

536 To account for this variability, we constructed a parameter distribution for
537 Km values based on diverse biological information. First, we chose a log-normal
538 distribution to guarantee positive Km values (Fig. 3): $Km_i \sim \log\mathcal{N}(\mu_{Km}, \sigma_{Km}^2)$,
539 where the mean μ_{Km} is set to the empirical median value of 13 different Km values
540 estimated from experimental data (Jeske et al., 2018; Jiang and Belasco, 2004; Kim
541 et al., 2004; Kime et al., 2008, 2010) (see also Table B.1 for some values). The
542 dispersion of these data did not reflect the expected variability of Km values *in*
543 *vivo*. We thus chose the standard deviation σ_{Km} such that it mirrors the variability
544 of mRNA concentrations measured experimentally: $\sigma_{Km} = \sigma_{m0}$, similarly to what
545 is found generally for many enzymes and their substrates (e.g. Bennett et al., 2009).
546 The chosen k_{cat} and Km_i values result in a mean catalytic efficiency constant of
547 $6 \cdot 10^5 \text{ s}^{-1}\text{M}^{-1}$, in the average of values determined experimentally for RNase E
548 (Table B.1). The mRNA concentrations at time 0, together with the RNase E
549 concentration, correspond to transcriptomics and proteomics data in (Valgepea
550 et al., 2013), which we discussed in Section 3.2. The mRNA concentrations form
551 a log-normal distribution illustrated on a logarithmic scale in Panel (a) of Fig. 3.
552 The corresponding distribution for Km values is shown in Panel (b). On the
553 logarithmic scale, the distribution is normal, while it is characterized by a longer
554 tail towards higher Km values on a linear scale. It reflects the proportion of
555 mRNAs potentially affected by specific regulations antagonizing RNase E (less
556 than 10% with the chosen variance). As well, an even smaller fraction of mRNAs
557 have low Km values, reflecting possible regulatory mechanisms activating mRNA
558 decay. This is altogether a reasonable assumption, given the similar fraction of
559 mRNAs shown or predicted to be regulated at the degradation level (Keseler et al.,
560 2017; Wright et al., 2014). The distribution of initial mRNA concentrations is also
561 characterized by a longer tail, where few mRNAs have high concentrations. Most
562 of them are present at low intracellular levels. For the catalytic constant, we used
563 the mean value estimated from experimental data obtained with various mRNAs
564 (Jeske et al., 2018). Overall, the distributions and parameter values set verify the
565 criteria of validity for the tQSSA described in Sections 3.3 and 3.4. Remember
566 that in these data, the individual mRNA concentrations are well below the RNase E
567 E concentration, while the total mRNA concentration is in large excess (Fig. 3).

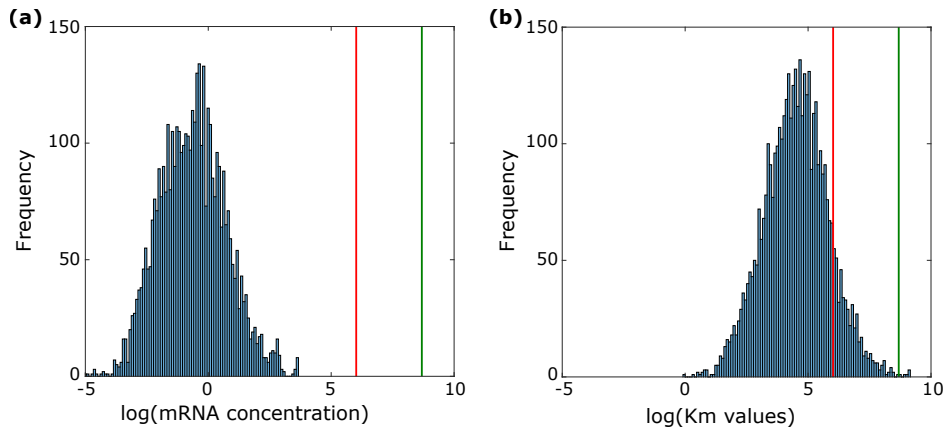


Figure 3: Log-normal distributions of initial concentrations (a) and Km values (b). The x-axes are on a logarithmic scale. The red and green lines denote the total concentrations of RNase E and mRNA, respectively.

568 *4.2. Competition between mRNAs slows down the degradation kinetics and*
 569 *increases the variability of progress curves*

570 With the parameter values and concentrations described above, we simulated
 571 the kinetic models of the isolated and competitive systems. The transcriptomics
 572 data used for the initial conditions includes information for 4312 mRNAs. We thus
 573 ran as many simulations. We took every time a Km value from the log-normal
 574 distribution as well as the fixed catalytic constant and enzyme concentration. The
 575 same values of parameters and initial conditions were used to simulate the models
 576 with and without competition. All simulations were performed with the function
 577 `ode15s` of Matlab (Mathworks).

578 Remember that the simulated models are approximated forms of the tQSSA,
 579 valid under the criteria described in Sections 3.3 and 3.4. We could not exclude
 580 that some combinations of parameters and initial concentrations may violate these
 581 criteria. Beforehand we thus compared the predictions generated by the various
 582 tQSSA models to make sure that approximations of poorest quality did not impact
 583 significantly the degradation profiles (see Appendix D.1). However, the strong re-
 584 semblance of the model predictions prompted us to use the approximated versions
 585 in the rest of the study.

586
 587 Fig. 4 describes the simulation results obtained with the approximated tQSSA
 588 models. Predicted mRNA concentrations are shown for the competitive system in
 589 Panel (a) and the isolated system in Panel (b) (see Fig. D.2 for a log scale repre-
 590 sentation of these results). The curves differ by the initial mRNA concentration and

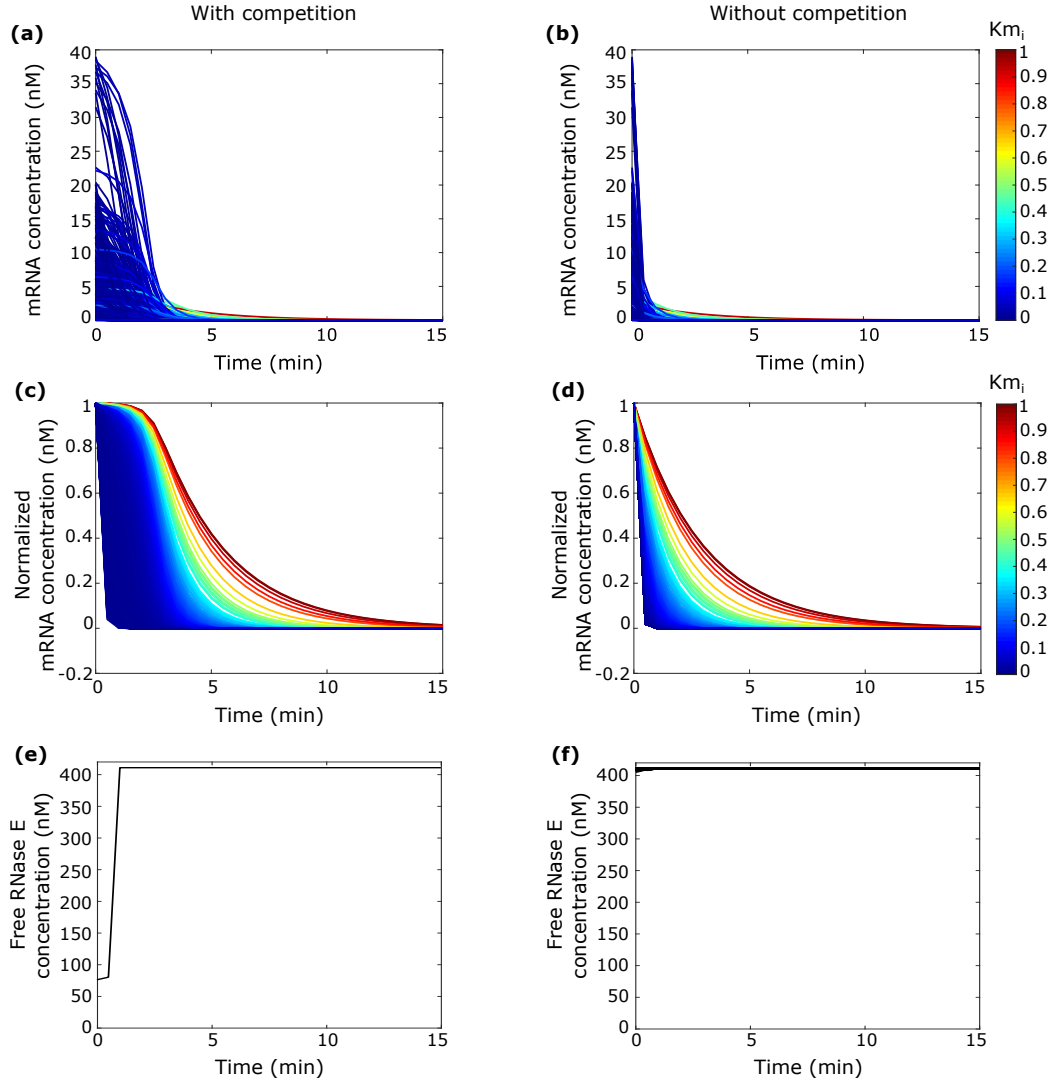


Figure 4: Numerical simulation of mRNA degradation kinetics in isolated and competitive systems. Predicted profiles for the competitive (a) and isolated (b) systems. The profiles are normalized to their respective initial concentrations for the competitive (c) and isolated (d) systems. Predicted free RNase E concentrations for (e) the competitive system ($E_{free} = E_0 - \sum_{i=1}^n c_i(t)$) and (f) the isolated one ($E_{i,free} = E_0 - c_i(t)$). 4312 curves are displayed in this case, due to the lack of coupling between mRNAs. The colour bars on the right side represent the normalized gradient of Km values, on a scale from zero (the minimal Km value) to one (maximal value).

591 the K_m value. However, the variability of the mRNA concentrations is such that
592 it hides the effect of differences of RNase E affinity, represented by curves from red
593 (high K_m values) to blue (low K_m). These differences are more visible in Panels
594 (c) and (d), where the same curves normalized to the initial mRNA concentrations
595 are shown. They differ by their K_m value only. A striking difference between the
596 isolated and competitive systems is the rapidity of the decay in the absence of com-
597 petition. After two minutes, all mRNAs are at least half degraded in the isolated
598 system (Panel (d)), whereas it takes almost five minutes to the competitive system
599 to reach the same state (Panel (c)). This slower rate of degradation is consistent
600 with measurements of mRNA half-lives in *E. coli* cells (Bernstein et al., 2002; Es-
601 querré et al., 2014). For instance in Esquerré et al. (2014), mRNAs have median
602 half-lives ranging from 2.9 to 4.2 minutes in *E. coli* cells at various doubling rates.
603 This general slowdown of mRNA degradation results from the reduced RNase E
604 affinity in a competitive system compared to an isolated one (Section 3.4). This
605 can be easily seen in Fig. E.1, where the distribution at time 0 of the apparent
606 K_m values (including the competition term) is shifted to a higher median value
607 compared to the distribution of K_m values.

608

609 The competitive effects result in more variable and more non-linear degradation
610 profiles. Hence, the competition affects how degradation is launched. It starts im-
611 mediately in isolated systems while it is delayed in competitive ones (Fig. 4(a,b)).
612 This delay is slightly more pronounced with the approximated tQSSA, but still
613 present in the absence of approximation (see Fig. D.1 for comparison). It is there-
614 fore a feature of competing mRNAs. The occurrence of delays in mRNA degrada-
615 tion kinetics is a known phenomenon. The primary reason is the common use of
616 rifampicin as a drug to block the initiation of transcription (e.g. Chen et al., 2015).
617 Elongating RNA polymerase is insensitive to the drug and pursues transcription.
618 During a transient time, the transcription rate counterbalances the degradation
619 rate. It is thus expected that longer transcripts have longer delays before mRNA
620 levels start decreasing (Chen et al., 2015; Esquerré et al., 2015; Moffitt et al., 2016).
621 Are there other determinants to the delay before degradation?

622

623 In our study we have not modelled the delay explicitly, as least not the time
624 required for the completion of transcription. The predicted delay results from the
625 titration of RNase E by competing mRNAs. As shown in Panel (e), the intracellu-
626 lar pool of free RNase E is strongly depleted in the first minutes of the degradation
627 kinetics in the competitive system. While the enzyme level is indeed much higher
628 than those of individual mRNAs, the total mRNA concentration is bigger and the
629 formation of complexes between the enzyme and the mRNAs limits the enzyme
630 availability. This implies that sole mRNAs at high initial concentration or with

631 low K_m values are more likely to be degraded by this small enzymatic pool. The
 632 intracellular pool of RNase E raises to higher levels when mRNAs are degraded to
 633 a large extent. At this time of the degradation kinetics, RNase E is in excess and
 634 all mRNAs can be degraded. This is what happens during the whole kinetics for
 635 mRNAs in the isolated system, since the enzyme concentration is never limiting
 636 (Panel (f)). The mRNAs can all bind to RNase E and be degraded soon afterwards.

637
 638 Another striking difference is the variability of the degradation profiles driven
 639 by competing mRNAs (compare Panels (a) and (b) or (c) and (d)). Even though
 640 we set the variance of the K_m distribution to quite a large value, it is clearly
 641 not enough to produce a large diversity of curves in the isolated system. With
 642 the same parameters and initial concentrations, the introduction of the competi-
 643 tion term gives rise to curves with variable shapes. This is especially true for
 644 the curves in dark blue in Panel (d), characterized by low K_m values. Addition
 645 of the competition term spread them out, as can be seen in Panel (c). Cyan to
 646 red curves, characterized by a high K_m , are not scattered but simply shifted. The
 647 corresponding mRNAs seem merely to be stabilized.

648
 649 Where do these variability and increased non linearity come from? As can be
 650 seen in Panels (a) and (b) for both isolated and competitive systems, many mRNAs
 651 have a low initial concentration. Many of them have also higher K_m values, as
 652 shown in Panels (c) and (d) (lines coloured from cyan to red). In these conditions,
 653 the mRNA concentration becomes negligible with respect to the K_m and/or the
 654 RNase concentration: $m_{i0} \ll Km_i + E_0$. Therefore, the kinetics in Eq. 6 can be
 655 approximated by the following system for isolated mRNAs:

$$\frac{d}{dt}m_i(t) \approx \frac{k_{cat} \times E_0}{Km_i + E_0} \times m_i(t). \quad (11)$$

656 For mRNAs in competition, it becomes possible to approximate the degrada-
 657 tion kinetics in Eq. 10 by:

$$\frac{d}{dt}m_i(t) \approx \frac{k_{cat} \times E_0}{Km_i \left(1 + \sum_{j \neq i} \frac{m_j(t)}{Km_j} \right) + E_0} \times m_i(t). \quad (12)$$

658 In both expressions, the degradation rate varies linearly with the mRNA con-
 659 centration. Note as a side comment that the solution of these ODEs is an expo-
 660 nential function comparable to the classical exponential model used to determine
 661 mRNA half-life (see Eq. 2). It is thus appropriate to fit the degradation profiles of

662 these particular mRNAs (higher K_m and/or lower initial concentration) with an
663 exponential model. The decrease of enzyme affinity resulting from the increased
664 apparent K_m value in the competitive system (Fig. E.1(a)) globally shifts the
665 curves to the right compared to the isolated system (look for instance at the cyan
666 to red curves in Panel (c) versus (d)). All mRNAs with higher K_m and/or lower
667 initial concentrations will react in the same manner. While they tend to be stable
668 in the isolated system, competition stabilizes them even more.

669
670 The situation is different for mRNAs characterized by higher initial concentra-
671 tions and/or lower K_m values. In these conditions, the approximation in Eqs. 11
672 and 12 does not hold any more. RNase E is closer to saturation at the beginning
673 of the degradation kinetics (see Fig. 4), the substrates start to compete and their
674 degradation rates depend on each other. The degradation rate is no longer linear
675 in the mRNA concentration and the non linearity is amplified by the multiplication
676 of the K_m value with the competitive term. We thus expect that these mRNAs re-
677 act differently to the competition. This is visible in Fig. E.1(b), where normalized
678 values of the K_m and apparent K_m for each mRNA are compared. We observe the
679 global rescaling of the apparent K_m values at time 0 in the competitive system.
680 However, for a non negligible part of the mRNAs, the trend of the rescaling is
681 different. mRNAs with higher K_m values in the isolated system can have lower
682 apparent K_m values in the competitive system. It is only later in the kinetics,
683 when mRNAs are degraded in large parts, that the curves for the isolated and
684 competitive systems are more alike. In these conditions, the mRNA concentration
685 becomes negligible. The degradation kinetics become again linear in the mRNA
686 concentration and can be approximated by the simplified expressions in Eqs. 11
687 and 12.

688
689 In summary, competition between mRNAs acts globally on mRNA decay by
690 decreasing RNase E affinity for its substrates and by retarding the onset of degra-
691 dation. It also acts on each mRNA individually. To better understand how the
692 own characteristics of mRNAs in terms of enzyme affinity and initial concentra-
693 tions lead to variable responses to competition, we determined rate sensitivity
694 coefficients for the two models, as we shall see in the following section.

695 **5. Determination of rate sensitivity coefficients disentangles the** 696 **effect of substrate concentration and enzyme affinity in compet-** 697 **itive systems**

698 In our models, mRNAs start to decay following the transcription arrest at time
699 zero. The initial velocity of the degradation reaction depends on the saturation

700 of RNase E. Any change in the initial concentrations of mRNAs and the enzyme
701 affinity is expected to affect the degree of saturation. This is exactly what bac-
702 teria experience in nature. They constantly adjust their growth rate to changing
703 environmental conditions. This involves a wide reorganization of gene expression,
704 which includes, among others, changes in mRNA abundance and half-life resulting
705 notably from post-transcriptional regulations (see Bernstein et al., 2004; Esquerré
706 et al., 2014, for instance). The latter affect the enzyme affinity for its substrates in
707 our modelling framework. The consequence is that mRNA stabilities should react
708 differently to these changes according to our simulation results in Section 4.2.

709
710 The determination of scaled rate sensitivity coefficients allow assessing how
711 changes of initial concentrations and RNase E affinity impact the degradation
712 rates. For each model, we derived such a coefficient for the initial velocity, by
713 determining the scaled change of the initial degradation rate of each mRNA i
714 upon a variation of mRNA concentrations at time 0 or of Km value. These coef-
715 ficients are the equivalent of the elasticities and control coefficients determined at
716 steady state in Metabolic Control Analysis (Heinrich and Schuster, 1996; Ingalls
717 and Sauro, 2003). Their analytical expressions are shown in Table 1.

718
719 We first examined how changing the initial concentration (m_{i0}) or Km value
720 (Km_i) of a messenger RNA i affects the initial velocity (v_i) of its degradation
721 reaction. The sign of the analytical expressions of the response coefficients in
722 Table 1 shows that the direction of the change is the same in both isolated and
723 competitive systems: increasing the initial concentration destabilizes the mRNA
724 ($R_{m_i}^{v_i} \geq 0$), while increasing the Km value (and thus decreasing the enzyme affin-
725 ity) stabilizes it ($R_{Km_i}^{v_i} \leq 0$). However, the amplitude of the change may differ
726 between both systems. We quantified it, by evaluating the analytical expressions
727 of the response coefficients for the various pairs of mRNA concentration and Km
728 used for the numerical simulations in Section 4.2. The linear interpolations of the
729 coefficients are reported as contour plots in Fig. 5. We also displayed as points the
730 pairs of concentration and Km value used to generate the degradation profiles in
731 Section 4.2.

732
733 The response coefficients with respect to the change in mRNA concentrations
734 are close to unity for both models (see Panels (a) and (b)). This means that in-
735 creasing the initial concentration by 10 % results in a similar $\sim 10\%$ increase in the
736 rate of degradation and conversely, a decrease in the time at which mRNAs are half
737 degraded. The coefficients tend to be even higher for the competitive system. The
738 initial velocity of mRNA degradation is thus essentially determined by the initial
739 messenger concentration and this effect is reinforced in competitive systems. This

Table 1: Scaled rate sensitivity coefficients of the initial velocity v_i with respect to changes in initial mRNA concentrations and Km values.

Model	Coefficients
Isolated system (Eq. 6)	<p>Effect of changes of m_{i0} and Km_i on v_i:</p> $R_{m_i}^{v_i} = \frac{\partial v_i}{\partial m_{i0}} \frac{m_{i0}}{v_i} = \frac{Km_i + E_0}{Km_i + E_0 + m_{i0}}$ $R_{Km_i}^{v_i} = \frac{\partial v_i}{\partial Km_i} \frac{Km_i}{v_i} = \frac{-Km_i}{Km_i + E_0 + m_{i0}}$
	<p>Effect of changes of m_{j0} and Km_j on v_i:</p> $R_{m_j}^{v_i} = \frac{\partial v_i}{\partial m_{j0}} \frac{m_{j0}}{v_i} = 0$ $R_{Km_j}^{v_i} = \frac{\partial v_i}{\partial Km_j} \frac{Km_j}{v_i} = 0$
Competitive system (Eq. 10)	<p>Effect of changes of m_{i0} and Km_i on v_i:</p> $R_{m_i}^{v_i} = \frac{\partial v_i}{\partial m_{i0}} \frac{m_{i0}}{v_i} = \frac{Km_i \times \left(1 + \sum_{j \neq i} \frac{m_{j0}}{Km_j}\right) + E_0}{Km_i \times \left(1 + \sum_{j \neq i} \frac{m_{j0}}{Km_j}\right) + E_0 + m_{i0}}$ $R_{Km_i}^{v_i} = \frac{\partial v_i}{\partial Km_i} \frac{Km_i}{v_i} = \frac{-Km_i \times \left(1 + \sum_{j \neq i} \frac{m_{j0}}{Km_j}\right)}{Km_i \times \left(1 + \sum_{j \neq i} \frac{m_{j0}}{Km_j}\right) + E_0 + m_{i0}}$
	<p>Effect of changes of m_{j0} and Km_j on v_i:</p> $R_{m_j}^{v_i} = \frac{\partial v_i}{\partial m_{j0}} \frac{m_{j0}}{v_i} = \frac{-m_{j0} \times \frac{Km_i}{Km_j}}{Km_i \times \left(1 + \sum_{j \neq i} \frac{m_{j0}}{Km_j}\right) + E_0 + m_{i0}}$ $R_{Km_j}^{v_i} = \frac{\partial v_i}{\partial Km_j} \frac{Km_j}{v_i} = -R_{m_j}^{v_i}$

740 agrees well with experimental observations, where mRNA concentration has been
741 found negatively correlated with mRNA half time in *E. coli* and *L. lactis* bacteria
742 (Esquerré et al., 2015; Nouaille et al., 2017). To reach this conclusion, the authors
743 of these studies analysed large data sets previously obtained in these bacteria grow-
744 ing in environmental conditions leading to changes in mRNA concentrations and
745 half-lives. Increasing specifically the concentrations of four mRNAs by means of
746 inducible promoters elicited again the same negative relationship between mRNA
747 concentration and stability (Nouaille et al., 2017). Similarly to our observations,
748 the correlation is more pronounced at low to middle mRNA concentrations, but
749 less at high mRNA concentration ($R_{m_i}^{v_i}$ coefficients are a bit smaller).

750

751 We then studied how the isolated and competitive systems react to changes in
752 enzyme affinity. The corresponding response coefficients are shown in Panels (c)
753 and (d) of Fig. 5. For the pairs of initial concentration and Km value used for the
754 numerical simulations in Fig. 4, changing the Km value by 10% leads, on average,
755 to a 3% decrease of the initial velocity in the isolated system ($R_{Km_i}^{v_i} \sim -0.3$) and
756 to a 9% decrease in the competitive system ($R_{Km_i}^{v_i} \sim -0.9$). This effect does not
757 depend on the initial mRNA concentration. It is stronger at higher Km, but the
758 range of Km values for which the system response is highly negative is much larger
759 in the competitive system than in the isolated one. It encompasses the majority of
760 the pairs of initial concentration and Km value used in the numerical simulations.

761

762 It is interesting to realize that initial concentrations impact the degradation
763 kinetics at two different levels in competitive systems. First of all, as described
764 above, they strongly influence mRNA stability due to the strong, positive response
765 of the degradation rate to changes of concentration. Secondly, they have an an-
766 tagonistic effect on the degradation rate in the competitive system, due to the
767 strong negative response to Km changes. This response to Km changes is low in
768 the isolated system, which implies that the enzyme affinity hardly compensates for
769 the effect of the initial concentration ($R_{Km_i}^{v_i} \sim -0.3$ and $R_{m_i}^{v_i} \sim 1$ on average for
770 the pairs of Km and initial concentration used in the numerical simulations). The
771 degradation kinetics of an isolated system is thus almost exclusively driven by the
772 initial mRNA concentration. Now, in the competitive system, the response coeffi-
773 cients are of opposite sign and similar amplitude ($R_{Km_i}^{v_i} \sim -0.9$ and $R_{m_i}^{v_i} \sim 1$ on
774 average). The combination of these two antagonistic effects explain the non linear-
775 ities observed in the predicted degradation curves in Fig. 4(a,c), in particular the
776 occurrence of delayed degradation when mRNAs compete between them. Indeed,
777 as long as the total mRNA concentration is high at the beginning of the kinetics,
778 it augments the apparent Km value to sufficiently high values to compensate for
779 the effect of the initial mRNA concentrations. RNase E is totally saturated and

780 the initial velocity is almost null. It is only when the total mRNA concentration
781 decreases significantly that the weight of the competitive term in Eq. 10 fades
782 away. RNase E is no longer saturated and the competitive system resembles the
783 isolated one, with less sensitivity to changes of enzyme affinity.

784

785 With these analyses, we were able to disentangle the contribution of Km and
786 mRNA concentration to the degradation kinetics in competitive systems. One
787 question remains open though. Since the degradation kinetics of all mRNAs are
788 coupled due to the competition, are they impacted by the cell composition in
789 mRNAs? The competition term in Eq. 10 includes the affinity of cell mRNAs j
790 different from the mRNA i of interest, as well as their concentration. Given that
791 there are 4312 different mRNAs in our biological system, the intuition would say
792 that the change of concentration or Km of a single mRNA should not affect the
793 degradation kinetics of another one. But how true is it? We further study this
794 question in the following section.

795 6. Effect of coupling on mRNA degradation kinetics

796 We analysed a new set of rate sensitivity coefficients to analyse how the changes
797 of concentration or Km value of another mRNA j affect the degradation kinetics of
798 a given mRNA i . The analytical expressions for these new coefficients are shown in
799 Table 1. The isolated system is characterized by the absence of coupling between
800 mRNAs. Consequently, the response coefficient to changes of Km value or initial
801 concentration of mRNA j is zero ($R_{m_j}^{v_i} = R_{K_{m_j}}^{v_i} = 0$). In the competitive system,
802 the analytical expression depends on the concentration of the other mRNA j and
803 the relative affinities of mRNAs j and i . The sign of the response coefficients $R_{m_j}^{v_i}$
804 and $R_{K_{m_j}}^{v_i}$ is opposed to the previous coefficients $R_{m_i}^{v_i}$ and $R_{K_{m_i}}^{v_i}$. It shows that in-
805 creasing the initial concentration of mRNA j stabilizes mRNA i ($R_{m_j}^{v_i} \leq 0$), while
806 increasing the Km value of mRNA j (and thus decreasing the enzyme affinity)
807 destabilizes it ($R_{K_{m_j}}^{v_i} \geq 0$). As previously, this is a matter of enzyme titration. If
808 a given mRNA j titrates more RNase E due to a high initial concentration or low
809 Km value, less RNase E will be available for mRNA i , which is stabilized.

810

811 We evaluated the response coefficients by determining how a change of 10% of
812 the initial concentration or Km of each of the 4312 mRNAs j affects the initial
813 velocity of each of the 4311 other mRNAs i and j itself. The results are shown
814 as heatmaps in Fig. F.1. In most cases, the mRNA j marginally affects the other
815 mRNAs (response coefficients close to zero, see the yellow area in Panel (b) for
816 $R_{m_j}^{v_i}$ and the dark blue area in Panel (c) for $R_{K_{m_j}}^{v_i}$). However, when it does impact
817 the initial velocity, it does so for all mRNAs i (see horizontal lines coloured from

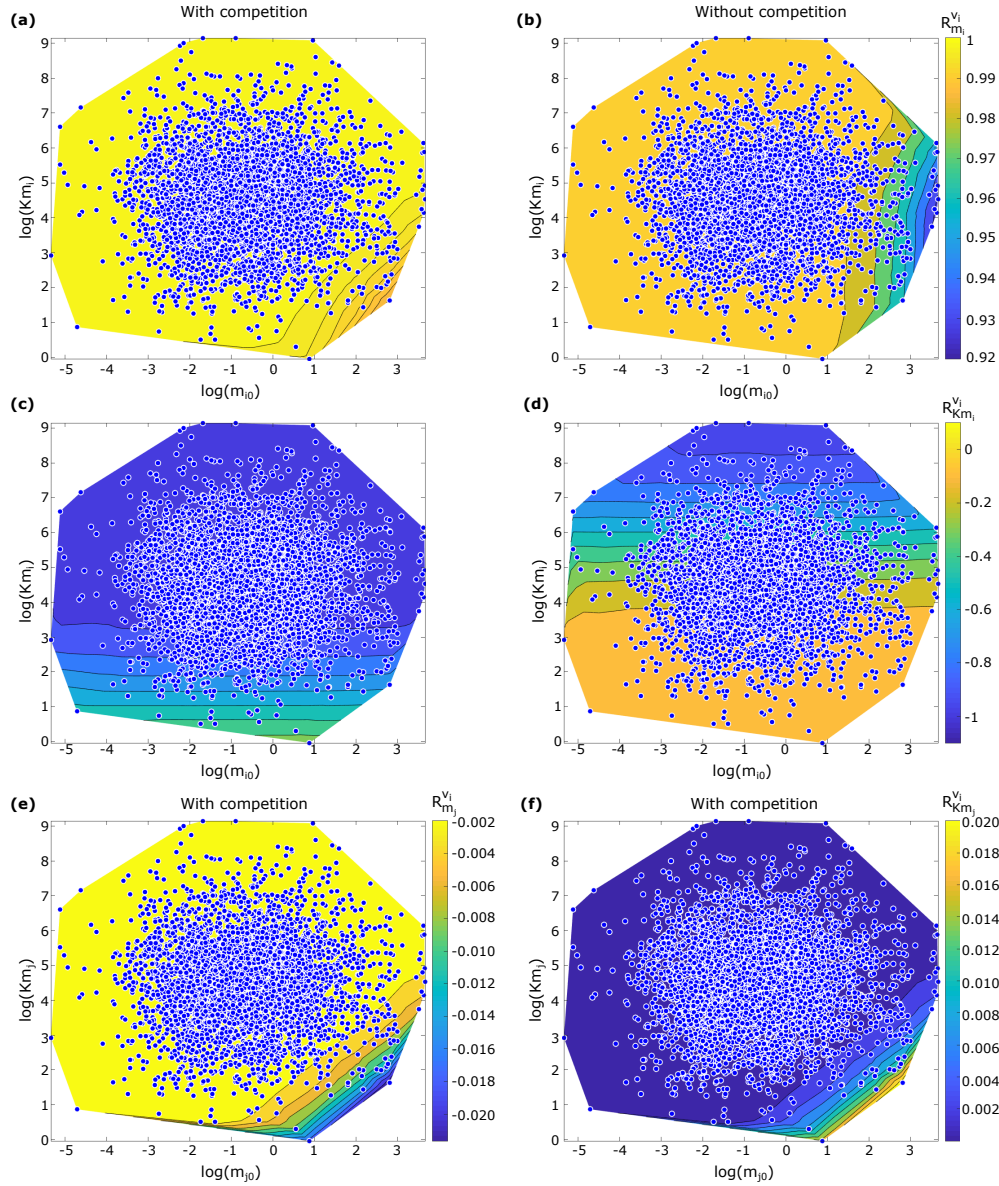


Figure 5: Scaled rate sensitivity coefficients for the initial velocity of mRNA i degradation. The points correspond to the pairs of initial concentration and K_m used in the numerical simulations in Fig. 4. For each pair, the contour plots display by means of linear interpolation the corresponding response coefficients with respect to (a) the initial concentrations ($R_{m_i}^{v_i}$) or (c) the K_m ($R_{K m_i}^{v_i}$), in a competitive system or in the isolated system ((b) and (d), respectively). Colour bars indicate the value of the elasticities. Panels (e) and (f) display the median response coefficients to changes of mRNA j concentration ($R_{m_j}^{v_i}$) or K_m ($R_{K m_j}^{v_i}$), respectively. The x- and y-axes are on a logarithmic scale.

818 orange to blue in Panel (b) of Fig. F.1, and from yellow to cyan in Panel (c)).
 819 To facilitate the analysis of the response coefficients, we thus took the median
 820 response coefficients of all mRNAs i to a change of either the Km value or the
 821 initial concentration of a given mRNA j (Fig. F.1). They express how changing
 822 the characteristics of mRNA j impacts the average mRNA i . The resulting co-
 823 efficients are shown in Panels (e) and (f) of Fig. 5. Each point (corresponding
 824 to a pair of initial concentration and Km value from the numerical simulations in
 825 Fig. 4) represents a given mRNA j . The response coefficients are way smaller than
 826 their counterparts $R_{m_i}^{v_i}$ and $R_{Km_i}^{v_i}$ in Panels (a) and (c), because they only concern
 827 the effect of an external mRNA j on the degradation of the average mRNA i .
 828 But interestingly, they are not negligible. The competitive effect is the strongest
 829 when the mRNA j has a high concentration or a low Km value. Increasing its
 830 concentration by 10% in this case reduces by 0.2% the initial velocity of mRNA
 831 i degradation ($R_{m_j}^{v_i} \sim -0.02$; Panel (e)). The effect is exactly the opposite when
 832 increasing the Km by 10%. This stimulates the initial degradation rate of the av-
 833 erage mRNA i by 0.2% ($R_{Km_j}^{v_i} \sim 0.02$; Panel (f)) and reduces the time at which it
 834 is half degraded. Hence, a highly competitive mRNA, which titrates more RNase
 835 E due to a high initial concentration or a low Km value, can affect the degradation
 836 rate of all cell mRNAs, with an average reduction of 0.2% of the velocity.

837

838 The competing effects that mRNAs exert on each other appear limited at first
 839 glance. However, these effects do exist whenever a single competing mRNA is
 840 considered and could be even stronger if several competing mRNAs are subject to
 841 changes. Indeed mRNA abundances and half-lives are known to massively adjust
 842 to environmental conditions (see Bernstein et al., 2004; Schneider et al., 1999, for
 843 instance). More precisely, modifications of the total mRNA concentration and the
 844 relative abundance of individual mRNAs have been observed. Changes in enzyme
 845 affinity are also expected for mRNAs specifically regulated by small RNAs and
 846 other post-transcriptional regulations. All these combined changes should affect
 847 the decay of all cell mRNAs according to our computed response coefficients. The
 848 global increase of the total mRNA concentration globally decrease the enzyme
 849 affinity, leading to a global but non uniform decrease of the individual degradation
 850 rates, since they are sensitive to various degrees to changes of Km values as we
 851 have seen in Panel (c). Among these mRNAs, those with the lowest Km values
 852 ($Km_i < Km_j$) and/or the highest initial concentrations ($m_{i0} > m_j$) are less
 853 sensitive to changes in the competing mRNA pool, because they are saturated by
 854 RNase E (Panels (a) and (c)). They behave similarly to mRNAs in an isolated
 855 system. However, the vast majority of cell mRNAs has a low concentration (see
 856 Fig. 3(a)) and most likely also a relatively weak affinity (Fig. 3(b)), such that they
 857 are not saturated by RNase E. Consequently, it is well possible that a majority of

858 cell mRNAs can be significantly affected by changes in competing mRNA pools, in
859 particular if the latter are highly concentrated and/or affine for RNase E (panels
860 (e) and (f)).

861 7. Discussion

862
863 We have developed in this study a mechanistic model of the coupled degrada-
864 tion of all cell mRNAs. The model represents a compromise in terms of complexity
865 and biological realism. Its predictions can be compared directly to degradation
866 profiles obtained experimentally. We hence assimilated the degradation mecha-
867 nism by the degradosome machinery to a macro-reaction catalysed by RNase E.
868 Literature data motivated the use of the tQSSA form of the Michaelis-Menten
869 equation for describing the degradation kinetics. We further approximated the
870 tQSSA model by extending previous work by Pedersen et al. (2007) and Tang
871 and Riley (2013). The resulting simplified model allows analysing the effect of
872 regulatory mechanisms on mRNA decay, which are difficult to test experimentally.
873 The possible implication of mRNA competition is one of them. While there is no
874 direct experimental proof for significant titration of RNase E, a body of evidences
875 – on its limited concentration relative that of mRNAs and its mean catalytic effi-
876 ciency – suggest that competition between mRNAs could well impact the mRNA
877 degradation kinetics (Section 3.4). We analysed the contribution of competition to
878 mRNA decay by means of numerical simulations and rate sensitivity coefficients,
879 based on carefully chosen parameter values and distributions. To the best of our
880 knowledge, this is the first study focusing on the role of competition in mRNA
881 turnover. A similar study was conducted on the maturation of transfer RNAs by
882 RNase P in conditions of limiting substrates (Yandek et al., 2013), but the number
883 of alternative substrates was low compared to our system. In addition the authors
884 of the study opted for the classical sQSSA form of the Michaelis-Menten frame-
885 work, which would not be suitable in our case, given its limits of validity.

886
887 Our results provide a plausible explanation to the observed delays and variable
888 degradation profiles in experimental studies. Under the effect of competition, the
889 profiles vary from seemingly exponential to more linear profiles. Such diversity is
890 difficult to reproduce in the absence of competition, while it is observed exper-
891 imentally (e.g., see Fig. A.1). The explanation lies in the titration of RNase E
892 at the beginning of the kinetics and as long as the total mRNA concentration re-
893 mains sufficiently high, which delays the onset of degradation. During this period
894 of time, mRNAs compete between them. The consequence is that the degradation
895 rate varies along time, from zero during the delay to maximal when free RNase E

896 is available, and back to zero towards the end of the kinetics. Such variation is
897 visible in experimental data (e.g., see Fig. A.1).

898

899 The lag effect caused by mRNA competition is a striking result. Residual tran-
900 scription is generally associated with delayed degradation, in particular for long
901 genes or genes towards the 3' end of operons (Chen et al., 2015). Could mRNA
902 competition be an additional mechanism? In the absence of direct evidence of
903 this phenomenon, through measurements of the free or bound concentration of
904 RNase E for instance, we cannot answer formally the question. However, an anal-
905 ysis of available dynamical transcriptomics data in *E. coli* indicates that residual
906 transcription alone does not suffice to explain the duration of the delay before
907 degradation kicks in (see Appendix G for details). We estimated the delay before
908 degradation for 3140 mRNAs of this data set (Esquerré et al., 2014), as well as
909 the time needed to transcribe each of them. In the absence of information on the
910 position of RNA polymerase at the time of rifampicin addition, determining the
911 time needed for transcribing an entire mRNA gives an upper bound to the residual
912 transcription time. Among the 2454 mRNAs that are not immediately degraded
913 after rifampicin addition, 51% of them have a delay before degradation larger than
914 the time needed for transcription. The delay is even twice larger for 21% of them
915 (Fig. G.2). While this quick analysis clearly underestimates the number of mRNAs
916 for which the transcription elongation takes a shorter time than the delay before
917 degradation, it indicates that residual transcription is not the sole determinant
918 for the delay in the data set studied. Competition between mRNAs could well be
919 another one.

920

921 The competition explains also the negative correlation observed between mRNA
922 half-life and concentration (Esquerré et al., 2015; Nouaille et al., 2017). Our model
923 has the advantage that it provides a mechanistic interpretation to the correlation,
924 through the coupling of the degradation kinetics of each mRNA. This results from
925 the fact that the competition acts at two different levels. First of all, the degra-
926 dation rate and thus the time at which the mRNA is half degraded is extremely
927 sensitive to mRNA concentration (Fig. 5(a)). This explains why the correlation
928 is the highest in the experimental data, in particular for mRNAs with low to in-
929 termediate concentrations (Nouaille et al., 2017). At higher mRNA levels, the
930 degradation rate becomes less sensitive to the concentrations while it can be still
931 strongly sensitive to the K_m values (Fig. 5(a,b)). This is where the correlation
932 between half-life and concentration is smaller: the mRNA half-lives no longer vary
933 with high mRNA concentrations.

934

935 Our simulation results and the response coefficients show that mRNA compe-

936 titation amplifies the effect of the K_m value in the degradation kinetics. mRNAs
937 that have intermediate to low affinities compete for binding to RNase E. The less
938 affine mRNAs will have less chance to be degraded: the competition term in their
939 apparent K_m value in Eq. 10 increases due to the presence of competing mRNAs
940 with higher affinities (the ratio $\sum_{j \neq i} \frac{m_j(t)}{K_{m_i}}$ takes higher values). This results in
941 a higher apparent K_m reflecting a stabilisation of these mRNAs (Fig. E.1(b)).
942 Hence, the more stable mRNAs are stabilized by competition. On the contrary,
943 the most affine mRNAs are saturated by RNase E, in both isolated and competi-
944 tive systems. They are among the less sensitive to the competition and can bind to
945 the low enzyme levels. The ratio $\sum_{j \neq i} \frac{m_j(t)}{K_{m_i}}$ in the competition term is among the
946 smallest throughout the population of mRNAs, because the competing mRNAs
947 have higher affinities. These mRNAs will have the smallest apparent K_m values
948 among the population of mRNAs (Fig. E.1(b)). The consequence is that these
949 unstable mRNAs in the isolated system are destabilized by competing mRNAs in
950 the competitive system.

951

952 By affecting differently the mRNAs, the competition brings about a diversity of
953 effects that is responsible for the larger variability of degradation profiles in a com-
954 petitive system with respect to an isolated one. Surprisingly, a single mRNA can
955 affect the degradation profiles of the other cell mRNAs, provided it is sufficiently
956 concentrated or affine for RNase E. All these observations are interesting because
957 it implies that cells can efficiently control the stability of their entire population
958 of mRNAs through the sole use of a competitive mechanism and a limiting en-
959 zyme concentration. This suggests that mRNA competition allows cells to adjust
960 degradation to transcription. Similar coupling effects are observed in Eukaryotes
961 and Prokaryotes like *E. coli*. Buffering mechanisms against changes in mRNA sta-
962 bility or transcription ensure that intracellular levels of mRNAs are maintained
963 for instance, although the molecular mechanisms have not been fully elucidated
964 (Dori-Bachash et al. 2011, 2012; Esquerré et al. 2014; Sun et al. 2012; Shalem
965 et al. 2011; see Hartenian and Glaunsinger 2019 for review). In our simulation
966 results, the positive coupling between transcription and degradation results from
967 the higher probability that mRNAs with increased concentration will be degraded.
968 However, we also observe a counter-acting effect that negatively correlates tran-
969 scription and degradation rates. The increase of mRNA concentration through
970 transcription increases RNase E apparent affinity and slows down degradation,
971 although the amplitude of the effect varies between mRNAs.

972

973 The occurrence of non linearities resulting from enzyme titration is a well
974 studied phenomenon in biochemistry. It has been observed in many biological sys-
975 tems, ranging from the MAP kinases to transcription and translation (e.g. Buchler

976 and Cross, 2009; De Vos et al., 2011; Huang and Ferrell, 1996; Mehra and Hatz-
977 imanikatis, 2006). Quite often, this results in ultrasensitive responses. We have
978 not really observed such phenomenon in our simulation study. The response coef-
979 ficients that we determined from the pairs of K_m value and initial concentrations
980 used for the numerical simulations are generally between -1 and 1 . Sole responses
981 above one in absolute value reflect an ultrasensitive behaviour. Values slightly be-
982 low -1 were sometimes obtained in specific conditions, when the K_m value of more
983 affine mRNAs i was varied. This does not mean that no ultra-sensitivity occurs
984 in mRNA degradation since the amplitude of the response coefficients strongly
985 depends on the chosen parametrization.

986

987 While we were able to retrieve quite precise values for the enzyme concentra-
988 tion, the mRNA concentrations and the catalytic constant in the literature, this
989 prove to be more difficult for the K_m value. Available data for the enzyme affinity
990 were obtained with a limited number of substrates in (often) *in vitro* assays. While
991 this gave a possible average affinity of RNase E for its substrates, it did not reflect
992 the variety of cell mRNAs. The latter were expected having different affinities,
993 depending on their structural and sequence determinants, as well as their possi-
994 ble regulations by small RNAs and other regulatory proteins. This is the reason
995 why we chose a distribution of K_m as large as the distribution of measured initial
996 concentrations to take into account as much as possible these different situations.
997 This said, using different K_m distributions would only tune the amplitude of the
998 competition effect. Indeed there will be always an antagonism between the con-
999 tributions of initial concentrations and enzyme affinities to the competition effect.
1000 Depending on their relative distributions, one may become prevailing. In our sim-
1001 ulations, the choice of distributions with similar variances lead to contributions of
1002 initial concentrations and K_m of similar strength in many cases.

1003

1004 Estimating the K_m value from experimental data, and possibly also the cat-
1005 alytic constant, could help refine our analysis on the role of mRNA competition
1006 in mRNA decay. This is beyond the scope of this study and will be done else-
1007 where (T.A. Etienne, L. Girbal, M. Coccagn-Bousquet, D. Ropers, in prepara-
1008 tion). Using a total quasi-steady-state approximation rather than the classical
1009 quasi-steady-state approximation is known to improve the estimation of param-
1010 eter values by introducing the enzyme concentration in the equation (Choi et al.,
1011 2017). In addition to helping with the identifiability problems related to the use
1012 of Michaelis-Menten kinetics, estimating the parameter values of such competition
1013 model allows to determine the true value of the K_m and not an apparent constant
1014 that includes a competition term.

1015

1016 The model developed is sufficiently general to be applied to other organisms
1017 and regulatory mechanisms of mRNA degradation. For instance, the apparent K_m
1018 value in our equations may be extended to include regulations by small RNAs or
1019 the competition by stable RNAs, which are also known to be matured by RNase
1020 E. The fact that RNase E is active both in the cytoplasm and bound to the
1021 membrane as part of the degradosome allows to interpret the K_m in a different
1022 manner. It also reflects the diffusion of substrates to the membrane and allows
1023 to study the effect of substrate localization in the degradation kinetics (Tang and
1024 Riley, 2013; Tzafiriri et al., 2002). Overall, we believe that our mechanistic model
1025 of mRNA degradation and its regulation by competition and other mechanisms is
1026 an interesting alternative to the classically used exponential models.

1027 **Acknowledgements**

1028 This work was supported by the Agence Nationale de la Recherche under
1029 project RibEco (ANR-18-CE43-0010), as well as by the Institut National de la
1030 Recherche Agronomique and Inria, from which T.A.E received a doctoral fellow-
1031 ship. The authors thank Hidde de Jong and Marco Mauri (Ibis, Inria) for dis-
1032 cussions, and Laurence Girbal (TBI, CNRS) for discussions as well as comments
1033 on a previous version of the manuscript. The authors also thank an anonymous
1034 reviewer for helpful comments.

1035 **Appendix A. Example of observed degradation kinetics**

1036 We illustrate the type of degradation profiles obtained experimentally with
1037 data obtained for mRNAs in *E. coli* cells growing at 0.4 h^{-1} in continuous cultures.
1038 We display in Fig. A.1 21 degradation profiles out of the 4254 profiles obtained in
1039 (Esquerré et al., 2014).

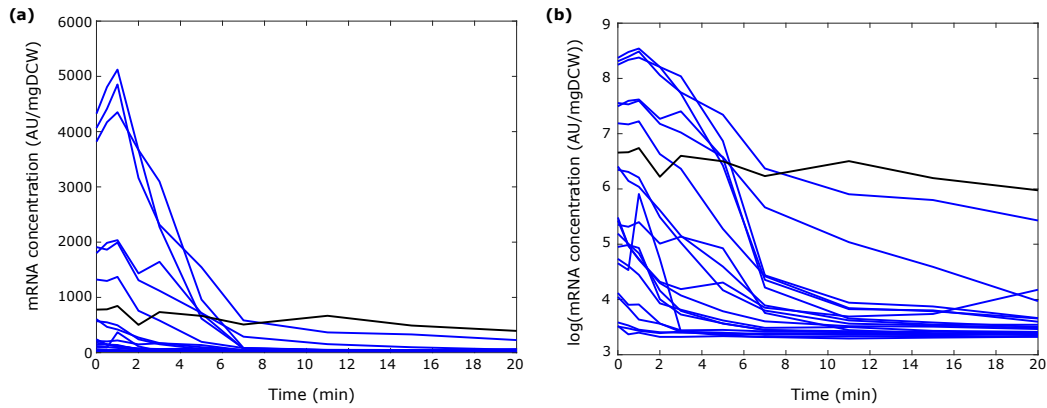


Figure A.1: Experimental monitoring of mRNA decay in *E. coli* cells growing in continuous culture at 0.4 h^{-1} . For readability, only 21 out of the 4254 generated profiles are displayed, both on linear (a) and semi-logarithmic (b) scales. At time 0 of the experiment, rifampicin was added to the culture and residual mRNA concentrations were quantified by DNA micro-arrays. Data were taken from (Esquerré et al., 2013). After delays of various duration, most mRNAs have a degradation kinetics resembling an exponential decay (blue curves), while other mRNAs can be slowly decaying, like the murein lipoprotein mRNA *lpp* (black curve).

1040 **Appendix B. Kinetic parameters of RNase E**

Table B.1: Catalytic efficiency of RNase E. Kinetic parameters k_{cat} and K_m were estimated from the same assays.

References: (1) - Jiang and Belasco (2004); (2) -Kim et al. (2004)

Ref.	Experimental conditions	Substrates	k_{cat} (s^{-1})	K_m (M)	k_{cat}/K_m ($M^{-1}\cdot s^{-1}$)
(1)	pH 7.5, 25°C, recombinant N-terminal domain	5' hydroxylated fluorogenic oligonucleotide	0.015	$3.3 \cdot 10^{-7}$	45455
(1)	pH 7.5, 25°C, recombinant N-terminal domain	5' monophosphorylated fluorogenic oligonucleotide	0.014	$2.3 \cdot 10^{-7}$	60870
(2)	pH 7.5, 30°C	AAUUU-containing RNA oligonucleotide	0.192	$7.3 \cdot 10^{-7}$	263,014
(2)	pH 7.5, 30°C	CAUUU-containing RNA oligonucleotide	0.150	$4.6 \cdot 10^{-7}$	326,087
(2)	pH 7.5, 30°C	GAUUU-containing RNA oligonucleotide	0.765	$1.2 \cdot 10^{-6}$	616,935
(2)	pH 7.5, 30°C	GUUUU-containing RNA oligonucleotide	0.121	$3.7 \cdot 10^{-7}$	327,027
(2)	pH 7.5, 30°C	UAUUU-containing RNA oligonucleotide	0.209	$8.1 \cdot 10^{-7}$	258,025
(2)	pH 7.5, 30°C	UUUUU-containing RNA oligonucleotide	0.023	$3.2 \cdot 10^{-6}$	71,875
		Mean	0.186 (11.2 min ⁻¹)	$5.6 \cdot 10^{-7}$	246,161
		Median	0.136 (8.1 min ⁻¹)	$4.1 \cdot 10^{-7}$	260,519
		Standard deviation	0.247	$3.4 \cdot 10^{-7}$	191,168

1041 **Appendix C. Development of the tQSSA model with competition**

1042 We first describe below the development of the mass-action law model in Equa-
 1043 tion 9 and its subsequent approximations into tQSSA and first-order tQSSA mod-
 1044 els.

1045 With $i = 1 \dots, n$, we can write the following mass-action law system:

$$\begin{aligned}
 \frac{dm_i(t)}{dt} &= -k_i^+ \times E_{free}(t) \times m_{i,free}(t) + k_i^- \times c_i(t) \\
 \frac{dE_{i,free}(t)}{dt} &= \sum_i^n (-k_i^+ \times E_{free}(t) \times m_{i,free}(t) + (k_i^- + k_{cat}) \times c_i(t)) \\
 \frac{dc_i(t)}{dt} &= k_i^+ \times [E_{free}(t) \times m_{i,free}(t)] - (k_i^- + k_{cat}) \times c_i(t) \quad (C.1) \\
 \frac{dP_i(t)}{dt} &= k_{cat} \times c_i(t),
 \end{aligned}$$

1046 with $i = 1 \dots, n$ and initial conditions at $t = 0$: $m_{i,free}(0), E_{free}(0), c_i(0), P_i(0)$.

1047
 1048

Using the conservation laws

$$\begin{aligned}
 \frac{dE_{i,free}(t)}{dt} + \sum_i^n \frac{dc_i(t)}{dt} &= 0 \Rightarrow E_{free}(t) + \sum_i^n c_i(t) = E_0 \\
 \frac{dm_{i,free}(t)}{dt} + \frac{dc_i(t)}{dt} + \frac{dP_i(t)}{dt} &= 0 \Rightarrow m_{i,free}(t) + c_i(t) + [P]_i(t) = m_{i,free}(t)
 \end{aligned}$$

1049 we can reduce the previous system:

$$\begin{aligned}
 \frac{dm_{i,free}(t)}{dt} &= -k_i^+ \times (E_0 - \sum_i^n c_i(t)) \times m_{i,free} + k_i^- \times c_i(t) \quad (C.2) \\
 \frac{dc_i(t)}{dt} &= k_i^+ \times (E_0 - \sum_i^n c_i(t)) \times m_{i,free}(t) - (k_i^- + k_{cat}) \times c_i(t)
 \end{aligned}$$

1050 We apply the total quasi-steady-state approximation $m_i(t) = m_{i,free}(t) + c_i(t)$
 1051 and obtain:

$$\begin{aligned}
 \frac{dm_i(t)}{dt} &= \frac{dm_{i,free}(t)}{dt} + \frac{dc_i(t)}{dt} = k_{cat} \times c_i(t) \quad (C.3) \\
 \frac{dc_i(t)}{dt} &= k_i^+ \times [(E_0 - \sum_i^n c_i(t)) \times (m_i(t) - c_i(t)) - Km_i \times c_i(t)],
 \end{aligned}$$

with Km_i the Michaelis constant:

$$Km_i = \frac{k_{cat} + k_i^-}{k_i^+} \quad (\text{C.4})$$

1052 We apply the quasi-steady-state assumption : $\frac{dc_i(t)}{dt} \sim 0$ and obtain:

$$(E_0 - \sum_i^n c_i(t)) \times (m_i(t) - c_i(t)) = Km_i \times c_i(t) \quad (\text{C.5})$$

and

$$c_i(t) = \frac{(E_0 - \sum_i^n c_i(t)) \times (m_i(t) - c_i(t))}{Km_i} \quad (\text{C.6})$$

1053 Two alternative methods have been proposed in the literature to solve the
 1054 non-linear system (C.6) for c_i . Tang and Riley (2013, 2017) use perturbation
 1055 theory applied to sQSSA to derive an approximated solution for the tQSSA system.
 1056 Pedersen et al. (2007) develop their approximation for a competing system with two
 1057 substrates by means of the total two Padé approximation. Applied to our system,
 1058 these approaches allow obtaining the following formulation for the approximated
 1059 concentration of complex c_i :

$$\frac{d}{dt}c_i(t) = \frac{E_0 \times m_i(t)}{Km_i \times \left(1 + \sum_{j \neq i} \frac{m_j(t)}{Km_j}\right) + E_0 + m_i(t)} \quad (\text{C.7})$$

1060 with $j = 1 \dots , n$.

1061 **Appendix D. Numerical simulations**

1062 *Appendix D.1. Numerical simulations will full system*

1063 To exclude the fact that poor combinations of mRNA concentrations and Km
 1064 values may violate the validity of the tQSSA approximation described in Sec-
 1065 tion 3.4, we simulated the full system in Eqs. 5 and 9 and compared the simu-
 1066 lation results with the profiles obtained with the approximated tQSSA in Fig. 4.
 1067 Simulation results are shown in Fig. D.1.

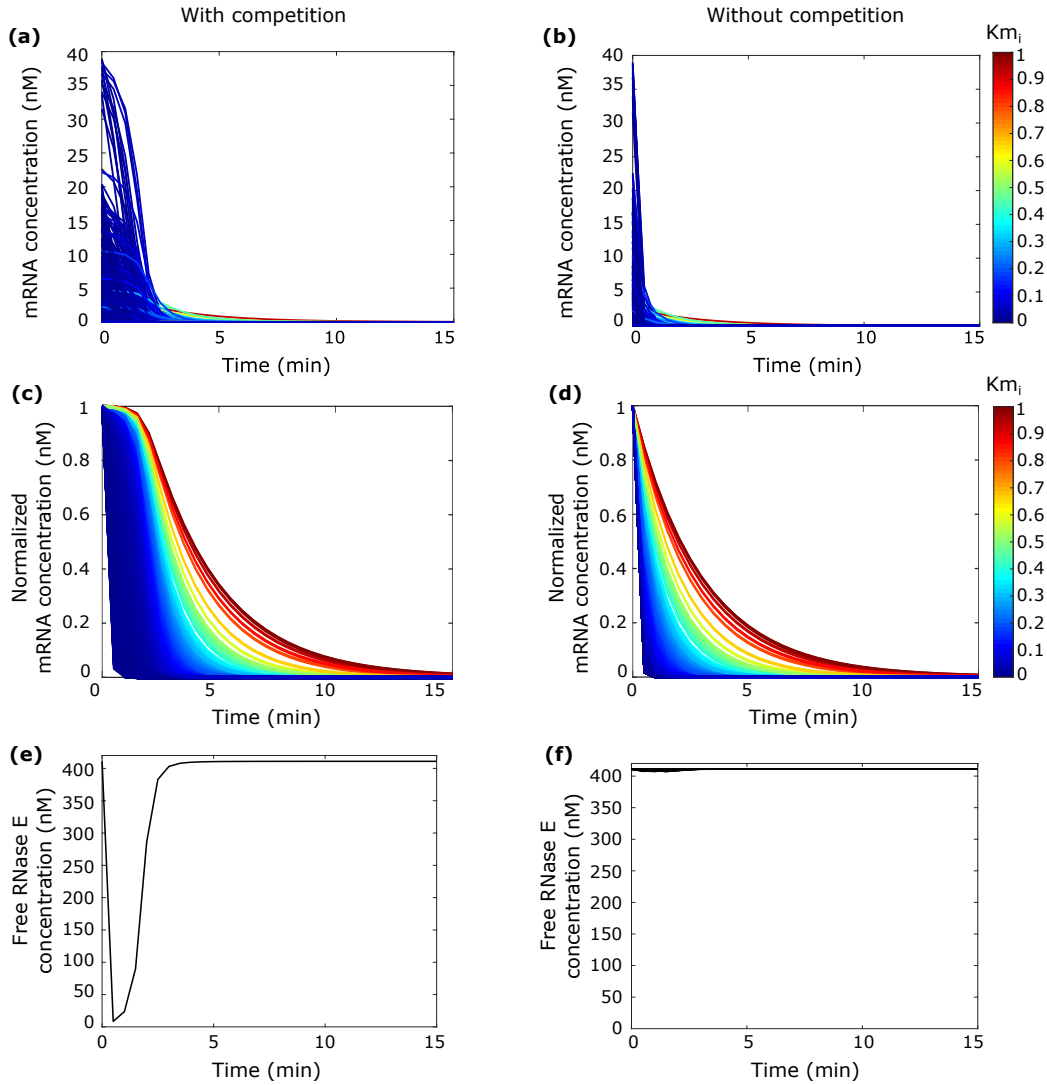


Figure D.1: Numerical simulation of mRNA degradation kinetics in isolated and competitive systems using Eqs. 5 and 9. Predicted profiles for the competitive (a) and isolated (b) systems. The profiles are normalized to their respective initial concentrations for the competitive (c) and isolated (d) systems. Predicted free RNase E concentrations for (e) the competitive system and (f) the isolated one. 4312 curves are displayed in this case, due to the lack of coupling between mRNAs. The colour bars on the right side represent the normalized gradient of K_m values, on a scale from zero (the minimal K_m value) to one (maximal value). Note that the total concentration of RNase E, but not the free concentration, is a variable in Eqs. 5 and 9. We thus calculated a posteriori the concentration of free RNase E from the total RNase E and complex concentrations. Since the model at time zero is not at steady state, we could not determine a steady-state value for the initial complex concentration, which would have given a more realistic value for the initial concentration of free RNase E. Instead, we used the same initial condition for the complex concentration as in the work of (Pedersen et al., 2007), with $c_i(0) = 0$. This effect is transitory only, since the free RNase E concentration predicted with Eq. 9 becomes quickly similar to that obtained with the approximated tQSSA model in Fig. 4(a).

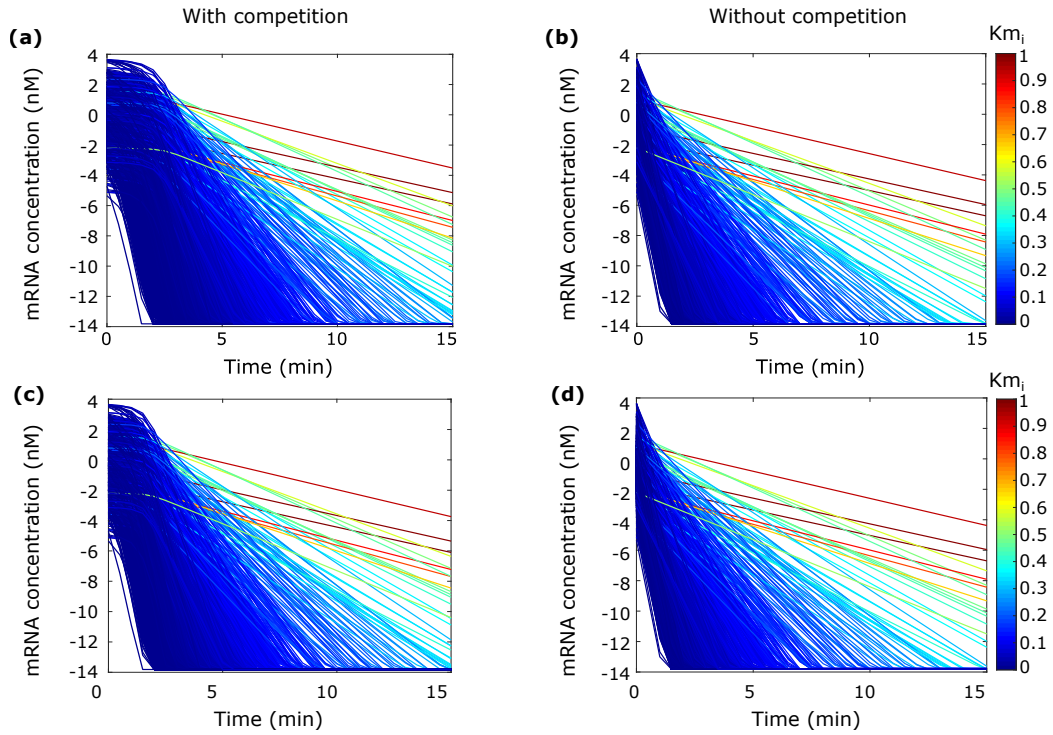


Figure D.2: Semi-logarithmic representation of simulation results shown in Figs. 4(a,b) (Panels (a) and (b)) and D.1(a,b) (Panels (c) and (d)). The predicted profiles for the competitive (a) and isolated (b) systems were obtained with the approximated tQSSA models (Eqs. 9 and 5, respectively). The predicted profiles obtained with the original models (Eqs. 10 and 6) are shown in Panels (c) and (d) respectively.

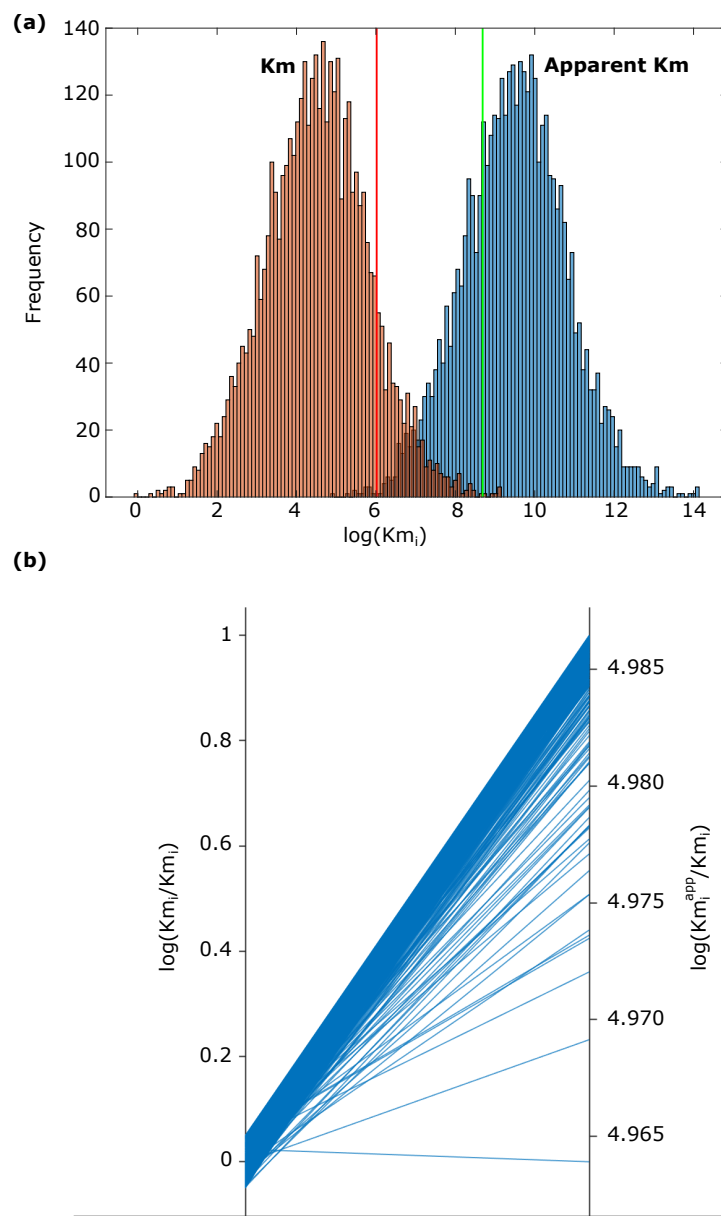


Figure E.1: Changes in enzyme affinity upon competition. (a) Log-normal distributions of Km (red) and apparent Km (blue) values. The x-axes are on a logarithmic scale. The red and green lines denote the total concentrations of RNase E and mRNA, respectively. (b) Parallel coordinate plot of Km_i (red) and Km_i^{app} values (blue) normalized to the Km value. Axes are on a logarithmic scale.

1068 *Appendix D.2. Log-scale representation of simulation results*

1069 **Appendix E. Changes of enzyme affinity upon competition**

1070 Competition rescale the enzyme affinity through the multiplication of the Km
1071 value with a term of competition. The amplitude of the changes is illustrated in
1072 Fig. E.1.

1073 **Appendix F. Heatmaps of rate sensitivity coefficients**

1074 In this section, we assess the effect of changing the initial concentration or Km
1075 value of a competing mRNA j on the initial velocity of the degradation of a given
1076 mRNA i . To that aim, we determine rate sensitivity coefficients for the effect of
1077 each of the 4312 mRNAs j on the degradation kinetics of each of the 4312 mRNAs
1078 i (they include the mRNA j itself). We obtain a square matrix of 4312×4312
1079 coefficients, represented as heatmap in Fig. F.1.

1080 **Appendix G. Contribution of transcription elongation to the delay 1081 before degradation**

1082 Elongation of transcription is known to delay degradation, but to which extent?
1083 We used a set of dynamic transcriptomics data from Esquerré et al. (2014) to
1084 answer the question. In this study, mRNA half-lives were determined in continuous
1085 cultures of *E. coli* cells growing at four different rates. We chose one condition
1086 (0.4 h^{-1}) and spline fitted the logarithm of the 4254 degradation profiles using
1087 the `smooth.spline` function of the R package `stat`. Further analysis was possible
1088 only for 3868 mRNAs, for which the spline fit was satisfactory and information
1089 on the gene length and promoter localization was available. For each of these
1090 3868 profiles, we determined the delay before degradation by simply finding the
1091 time point at which the sign of the first derivative of the spline function changes,
1092 from positive or null to negative due to the decrease of mRNA concentration. We
1093 observed the same phenomena as Chen et al. (2015) in their study: the size of
1094 mRNAs and their position towards the end of an operon increases the duration of
1095 the delay. This is illustrated in Figure G.1 in the case of the operon *nuo*. Genes
1096 at the beginning of the operon *nuo* have shorter delays before start of degradation
1097 than genes near the 3' end (Panel (b)). The same trend is observed when plotting
1098 the distance from the 5' end of the operon to the 3' end of each gene (Panel
1099 (c)). However, this is not a general rule. For instance, we noticed that many
1100 monocistronic mRNAs of low to medium size have also a delay.

1101 We then assessed the contribution of residual transcription to the total duration
1102 of the delay before degradation. In principle, this would require to know the

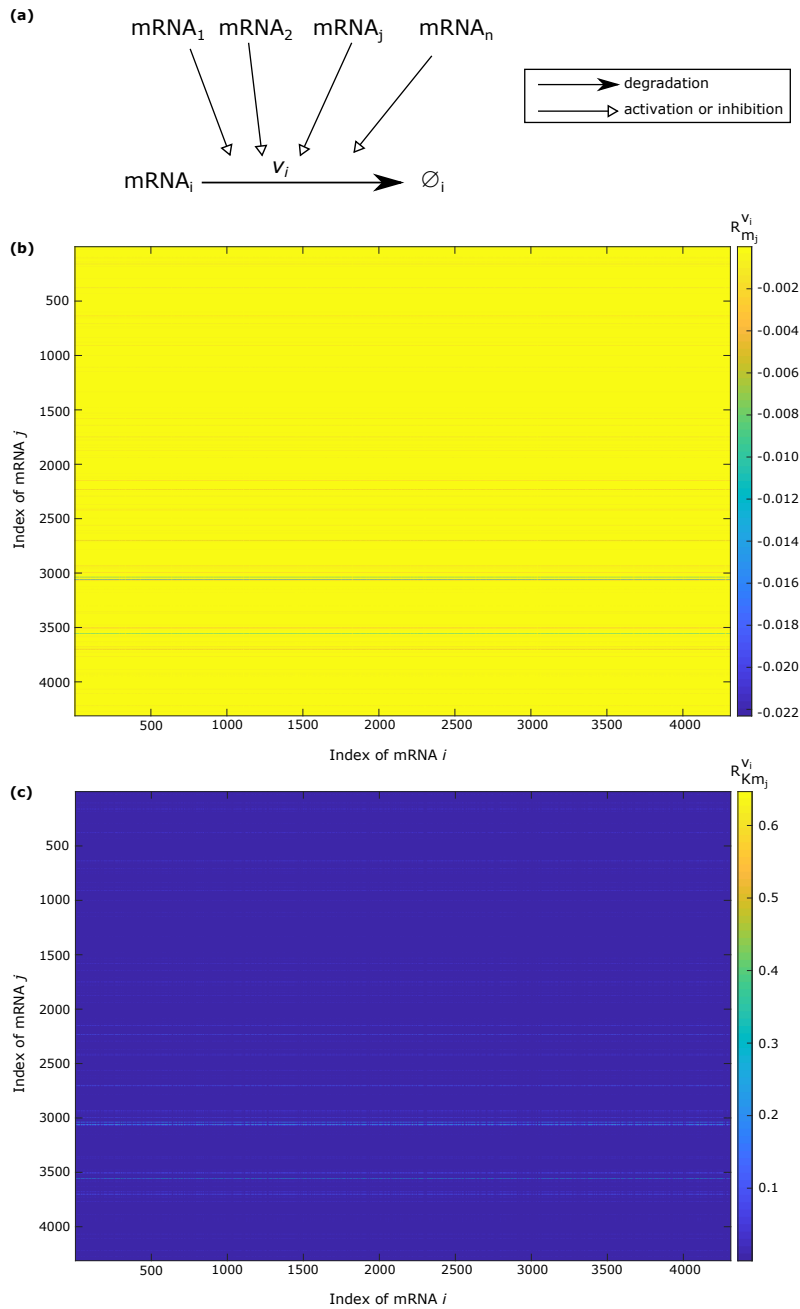


Figure F.1: Scaled rate sensitivity coefficients for the initial velocity of mRNA i degradation. (a) Schematic drawing of the coupling between the degradation of mRNA i and the other cell mRNAs j . We determined, for each of the 4312 *E. coli* mRNAs i , the effect of a 10% change in (b) the initial concentration and (c) the Km value of mRNA j on the initial degradation rate of each of the 4312 mRNAs i . Colour bars indicate the value of the response coefficients.

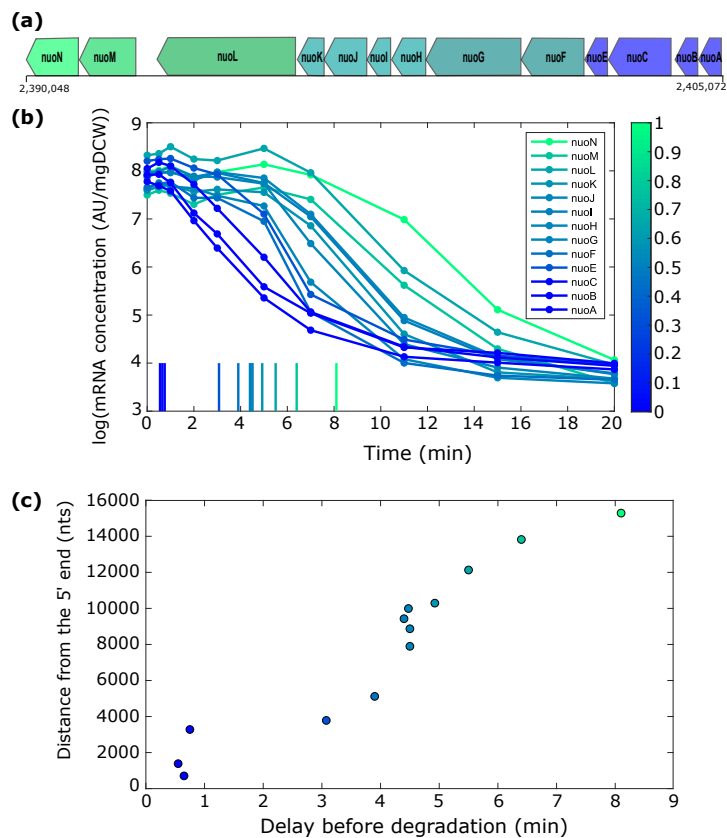


Figure G.1: The distance from the 5' end of the operon *nuo* scales proportionally to the duration of the delay before start of RNA degradation. (a) Organization of the *nuo* operon. Numbers indicate genome position in base. (b) RNA concentration over time of exponential phase MG1655 cells growing at 0.4 h^{-1} on a semilogarithmic scale. Vertical lines indicate the duration of the delay. (c) Delay before degradation increases with the distance of the gene transcript to the 5' end of the operon.

1103 position of RNA polymerase when rifampicin inhibits the holoenzyme. Such data
1104 is not available, which makes it impossible to determine the residual transcription
1105 time precisely. However, we can set an upper limit to this time, by determining the
1106 time needed to transcribe entire mRNAs. If this transcription time is smaller than
1107 the delay before degradation, this means that residual transcription cannot be the
1108 sole determinant of the delay. Results are more difficult to interpret when the
1109 maximal transcription time is larger than the delay before degradation. They can
1110 reflect co-transcriptional degradation as in (Chen et al., 2015) for instance, but also
1111 include false negative: mRNAs with low residual transcription time, but total gene
1112 transcription time larger than the delay, should be counted as mRNAs for which
1113 residual transcription is not the sole determinant of the delay. To determine the
1114 time needed for transcription, we multiplied the elongation rate of transcription
1115 determined at the genome scale by Chen and co-authors (25 nts/s on average),
1116 with the length of each mRNA. When a gene is located within an operon, we used
1117 the promoter operon to determine a maximal size for that mRNA. We focused on
1118 the 2454 out of 3868 mRNAs with a delay before the onset of degradation (the
1119 remaining 1414 are immediately degraded). As shown in Fig. G.2, 1255 out of
1120 2454 mRNAs have a delay before degradation larger than the maximal theoretical
1121 time needed for transcription (points in blue). 512 of them have a delay before
1122 degradation twice as large as the transcription time. Overall these results show
1123 that, for a vast majority of genes, transcription alone does not explain the whole
1124 duration of the delay with the transcription rate considered. This does not prove
1125 the role of competition experimentally, but does not exclude that this phenomenon
1126 could play a role in the retardation of degradation. Note we cannot rule out that
1127 heterogeneity in the polymerisation rate in transcription or in degradation may
1128 affect the estimated transcription times and delays before degradation. However,
1129 our analysis is based on population data for which information on heterogeneity
1130 is not available.

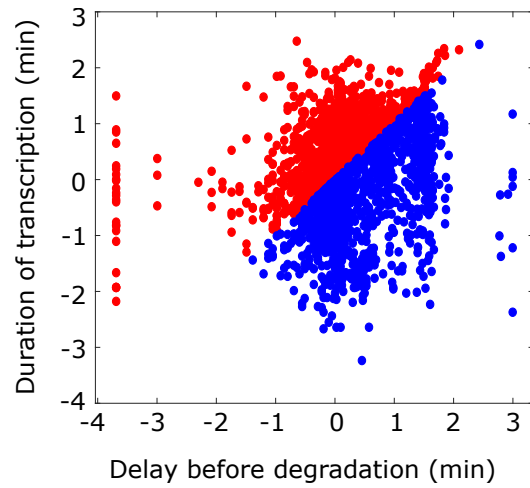


Figure G.2: Role of residual transcription in the retardation of degradation. On log scales and for each mRNA with a non negligible delay, the duration of transcription is plotted versus the delay before degradation. mRNAs with a delay higher than the time needed for transcription are displayed in blue and red, otherwise.

1131 **References**

- 1132 Albe, K.R., Butler, M.H., Wright, B.E., 1990. Cellular concentrations of enzymes
1133 and their substrates. *J Theor Biol* 143, 163–195.
- 1134 Bandyra, K.J., Wandzik, J.M., Luisi, B.F., 2018. Substrate recognition and au-
1135 toinhibition in the central ribonuclease RNase E. *Mol Cell* 72, 275–285.
- 1136 Bennett, B.D., Kimball, E.H., Gao, M., Osterhout, R., Van Dien, S.J., Rabinowitz,
1137 J.D., 2009. Absolute metabolite concentrations and implied enzyme active site
1138 occupancy in *Escherichia coli*. *Nat. Chem. Biol.* 5, 593–599.
- 1139 Bernstein, J.A., Khodursky, A.B., Lin, P.H., Lin-Chao, S., Cohen, S.N., 2002.
1140 Global analysis of mRNA decay and abundance in *Escherichia coli* at single-
1141 gene resolution using two-color fluorescent DNA microarrays. *Proc Natl Acad*
1142 *Sci USA* 99, 9697–9702.
- 1143 Bernstein, J.A., Lin, P.H., Cohen, S.N., Lin-Chao, S., 2004. Global analysis of
1144 *Escherichia coli* RNA degradosome function using DNA microarrays. *Proc Natl*
1145 *Acad Sci USA* 101, 2758–2763.
- 1146 Bobrovskyy, M., Vanderpool, C.K., Richards, G.R., 2015. Small RNAs regulate
1147 primary and secondary metabolism in Gram-negative bacteria, in: *Metabolism*
1148 *and Bacterial Pathogenesis*. American Society of Microbiology, pp. 59–94.
- 1149 Borghans, J.A.M., de Boer, R.J., Segel, L.A., 1996. Extending the quasi-steady
1150 state approximation by changing variables. *Bull Math Biol* 58, 43–63.
- 1151 Briggs, G.E., Haldane, J.B.S., 1925. A note on the kinetics of enzyme action.
1152 *Biochem J* 19, 338.
- 1153 Buchler, N.E., Cross, F.R., 2009. Protein sequestration generates a flexible ultra-
1154 sensitive response in a genetic network. *Mol Syst Biol* 5.
- 1155 Callaghan, A.J., Marcaida, M.J., Stead, J.A., McDowall, K.J., Scott, W.G., Luisi,
1156 B.F., 2005. Structure of *Escherichia coli* RNase E catalytic domain and impli-
1157 cations for RNA turnover. *Nature* 437, 1187.
- 1158 Carpousis, A.J., 2007. The RNA degradosome of *Escherichia coli*: an mRNA-
1159 degrading machine assembled on RNase E. *Annu Rev Microbiol* 61, 71–87.
- 1160 Carrier, T.A., Keasling, J., 1997. Mechanistic modeling of prokaryotic mRNA
1161 decay. *J Theor Biol* 189, 195–209.

- 1162 Celesnik, H., Deana, A., Belasco, J.G., 2007. Initiation of RNA decay in *Es-*
1163 *cherichia coli* by 5' pyrophosphate removal. *Mol Cell* 27, 79–90.
- 1164 Chao, Y., Li, L., Girodat, D., Förstner, K.U., Said, N., Corcoran, C., Śmiga,
1165 M., Papenfort, K., Reinhardt, R., Wieden, H.J., et al., 2017. *In vivo* cleavage
1166 map illuminates the central role of RNase E in coding and non-coding RNA
1167 pathways. *Mol Cell* 65, 39–51.
- 1168 Chen, H., Shiroguchi, K., Ge, H., Xie, X.S., 2015. Genome-wide study of mRNA
1169 degradation and transcript elongation in *Escherichia coli*. *Mol Syst Biol* 11,
1170 781.
- 1171 Choi, B., Rempala, G.A., Kim, J.K., 2017. Beyond the Michaelis-Menten equation:
1172 Accurate and efficient estimation of enzyme kinetic parameters. *Sci Rep* 7,
1173 17018.
- 1174 Clarke, J.E., Kime, L., Romero A, D., McDowall, K.J., 2014. Direct entry by
1175 RNase E is a major pathway for the degradation and processing of RNA in
1176 *Escherichia coli*. *Nucleic Acids Res* 42, 11733–11751.
- 1177 Cookson, N.A., Mather, W.H., Danino, T., Mondragón-Palomino, O., Williams,
1178 R.J., Tsimring, L.S., Hasty, J., 2011. Queueing up for enzymatic processing:
1179 correlated signaling through coupled degradation. *Mol Syst Biol* 7.
- 1180 Cornish-Bowden, A., 2013. The origins of enzyme kinetics. *FEBS Lett* 587, 2725–
1181 2730.
- 1182 Dar, D., Sorek, R., 2018. Extensive reshaping of bacterial operons by programmed
1183 mRNA decay. *PLoS Genet* 14, e1007354.
- 1184 De Vos, D., Bruggeman, F.J., Westerhoff, H.V., Bakker, B.M., 2011. How molec-
1185 ular competition influences fluxes in gene expression networks. *PloS One* 6,
1186 e28494.
- 1187 Deana, A., Belasco, J., 2005. Lost in translation: the influence of ribosomes on
1188 bacterial mRNA decay. *Genes Dev* 19, 2526–2533.
- 1189 Deana, A., Celesnik, H., Belasco, J.G., 2008. The bacterial enzyme RppH triggers
1190 messenger RNA degradation by 5' pyrophosphate removal. *Nature* 451, 355.
- 1191 Del Campo, C., Bartholomäus, A., Fedyunin, I., Ignatova, Z., 2015. Secondary
1192 structure across the bacterial transcriptome reveals versatile roles in mRNA
1193 regulation and function. *PLoS Genet* 11, e1005613.

- 1194 Deneke, C., Lipowsky, R., Valleriani, A., 2013. Effect of ribosome shielding on
1195 mRNA stability. *Phys Biol* 10, 046008.
- 1196 Dori-Bachash, M., Shalem, O., Manor, Y., Pilpel, Y., Tirosh, I., 2012. Widespread
1197 promoter-mediated coordination of transcription and mRNA degradation.
1198 *Genome Biol* 13, R114.
- 1199 Dori-Bachash, M., Shema, E., Tirosh, I., 2011. Coupled evolution of transcription
1200 and mRNA degradation. *PLoS Biol* 9, e1001106.
- 1201 Dressaire, C., Pobre, V., Laguerre, S., Girbal, L., Arraiano, C.M., Cocaign-
1202 Bousquet, M., 2018. PNPase is involved in the coordination of mRNA degrada-
1203 tion and expression in stationary phase cells of *Escherichia coli*. *BMC Genomics*
1204 19, 848.
- 1205 Esquerré, T., Laguerre, S., Turlan, C., Carpousis, A.J., Girbal, L., Cocaign-
1206 Bousquet, M., 2013. Dual role of transcription and transcript stability in the
1207 regulation of gene expression in *Escherichia coli* cells cultured on glucose at
1208 different growth rates. *Nucleic Acids Res* 42, 2460–2472.
- 1209 Esquerré, T., Laguerre, S., Turlan, C., Carpousis, A.J., Girbal, L., Cocaign-
1210 Bousquet, M., 2014. Dual role of transcription and transcript stability in the
1211 regulation of gene expression in *Escherichia coli* cells cultured on glucose at
1212 different growth rates. *Nucleic Acids Res* 42, 2460–2472.
- 1213 Esquerré, T., Moisan, A., Chiapello, H., Arike, L., Vilu, R., Gaspin, C., Cocaign-
1214 Bousquet, M., Girbal, L., 2015. Genome-wide investigation of mRNA lifetime
1215 determinants in *Escherichia coli* cells cultured at different growth rates. *BMC*
1216 *Genomics* 16, 275.
- 1217 Garrey, S.M., Mackie, G.A., 2011. Roles of the 5'-phosphate sensor domain in
1218 RNase E. *Mol Microbiol* 80, 1613–1624.
- 1219 Hartenian, E., Glaunsinger, B.A., 2019. Feedback to the central dogma: cyto-
1220 plasmic mRNA decay and transcription are interdependent processes. *Crit Rev*
1221 *Biochem Mol Biol* 54, 385–398.
- 1222 Heinrich, R., Schuster, S., 1996. *The Regulation of Cellular Systems*. Chapman
1223 and Hall. New-York.
- 1224 Huang, C.Y., Ferrell, J.E., 1996. Ultrasensitivity in the mitogen-activated protein
1225 kinase cascade. *Proc Natl Acad Sci USA* 93, 10078–10083.

- 1226 Huang, H., Liao, J., Stanley, N.C., 1998. Poly (A)-and poly (U)-specific RNA 3'
1227 tail shortening by *E. coli* ribonuclease E. *Nature* 391, 99.
- 1228 Hundt, S., Zaigler, A., Lange, C., Soppa, J., Klug, G., 2007. Global analysis of
1229 mRNA decay in *Halobacterium salinarum* NRC-1 at single-gene resolution using
1230 DNA microarrays. *J Bacteriol* 189, 6936–6944.
- 1231 Ingalls, B.P., Sauro, H.M., 2003. Sensitivity analysis of stoichiometric networks:
1232 an extension of metabolic control analysis to non-steady state trajectories. *J*
1233 *Theor Biol* 222, 23–36.
- 1234 Jain, C., Belasco, J., 1995a. Autoregulation of RNase E synthesis in *Escherichia*
1235 *coli.*, in: *Nucleic Acids Symp Series*, pp. 85–88.
- 1236 Jain, C., Belasco, J.G., 1995b. RNase E autoregulates its synthesis by controlling
1237 the degradation rate of its own mRNA in *Escherichia coli*: unusual sensitivity
1238 of the *rne* transcript to RNase E activity. *Genes & Dev* 9, 84–96.
- 1239 Jeske, L., Placzek, S., Schomburg, I., Chang, A., Schomburg, D., 2018. BRENDA
1240 in 2019: a European ELIXIR core data resource. *Nucleic Acids Res* 47, D542–
1241 D549.
- 1242 Jiang, X., Belasco, J.G., 2004. Catalytic activation of multimeric RNase E and
1243 RNase G by 5'-monophosphorylated RNA. *Proc Natl Acad Sci USA* 101, 9211–
1244 9216.
- 1245 Keseler, I.M., Mackie, A., Santos-Zavaleta, A., Billington, R., Bonavides-Martínez,
1246 C., Caspi, R., Fulcher, C., Gama-Castro, S., Kothari, A., Krummenacker, M.,
1247 et al., 2017. The EcoCyc database: reflecting new knowledge about *escherichia*
1248 *coli* K-12. *Nucleic Acids Res* 45, D543–D550.
- 1249 Kiel, C., Serrano, L., 2012. Challenges ahead in signal transduction: MAPK as an
1250 example. *Curr Opin Biotechnol* 23, 305–314.
- 1251 Kim, K.s., Sim, S., Ko, J.h., Cho, B., Lee, Y., 2004. Kinetic analysis of precursor
1252 M1 RNA molecules for exploring substrate specificity of the N-terminal catalytic
1253 half of RNase E. *J Biochem* 136, 693–699.
- 1254 Kim, Y., Andreu, M.J., Lim, B., Chung, K., Terayama, M., Jiménez, G., Berg,
1255 C.A., Lu, H., Shvartsman, S.Y., 2011. Gene regulation by MAPK substrate
1256 competition. *Dev Cell* 20, 880–887.

- 1257 Kim, Y., Coppey, M., Grossman, R., Ajuria, L., Jiménez, G., Paroush, Z., Shvarts-
1258 man, S.Y., 2010. MAPK substrate competition integrates patterning signals in
1259 the *Drosophila* embryo. *Curr Biol* 20, 446–451.
- 1260 Kime, L., Jourdan, S.S., McDowall, K.J., 2008. Identifying and characterizing
1261 substrates of the RNase E/G family of enzymes. *Methods Enzymol* 447, 215–
1262 241.
- 1263 Kime, L., Jourdan, S.S., Stead, J.A., Hidalgo-Sastre, A., McDowall, K.J., 2010.
1264 Rapid cleavage of RNA by RNase E in the absence of 5' monophosphate stim-
1265 ulation. *Mol Microbiol* 76, 590–604.
- 1266 Kushner, S.R., 2002. mRNA decay in *Escherichia coli* comes of age. *J Bacteriol*
1267 184, 4658–4665.
- 1268 Laguerre, S., González, I., Nouaille, S., Moisan, A., Villa-Vialaneix, N., Gaspin, C.,
1269 Bouvier, M., Carpousis, A.J., Coccagn-Bousquet, M., Girbal, L., 2018. Large-
1270 scale measurement of mRNA degradation in *Escherichia coli*: To delay or not
1271 to delay. *Methods Enzymol* 612, 47–66.
- 1272 Lee, K., Zhan, X., Gao, J., Qiu, J., Feng, Y., Meganathan, R., Cohen, S.N.,
1273 Georgiou, G., 2003. RraA: a protein inhibitor of RNase E activity that globally
1274 modulates RNA abundance in *E. coli*. *Cell* 114, 623–634.
- 1275 Legewie, S., Schoeberl, B., Blüthgen, N., Herzog, H., 2007. Competing docking
1276 interactions can bring about bistability in the mapk cascade. *Biophys J* 93,
1277 2279–2288.
- 1278 Luciano, D.J., Vasilyev, N., Richards, J., Serganov, A., Belasco, J.G., 2017. A
1279 novel RNA phosphorylation state enables 5' end-dependent degradation in *Es-*
1280 *cherichia coli*. *Mol Cell* 67, 44–54.
- 1281 Lugowski, A., Nicholson, B., Rissland, O.S., 2018. Determining mRNA half-lives
1282 on a transcriptome-wide scale. *Methods* 137, 90–98.
- 1283 Lykke-Andersen, S., Brodersen, D.E., Jensen, T.H., 2009. Origins and activities
1284 of the eukaryotic exosome. *J Cell Sci* 122, 1487–1494.
- 1285 Mackie, G.A., 1998. Ribonuclease E is a 5'-end-dependent endonuclease. *Nature*
1286 395, 720.
- 1287 Mackie, G.A., 2013. RNase E: at the interface of bacterial RNA processing and
1288 decay. *Nat Rev Microbiol* 11, 45.

- 1289 Marcaida, M.J., DePristo, M.A., Chandran, V., Carpousis, A.J., Luisi, B.F., 2006.
1290 The RNA degradosome: life in the fast lane of adaptive molecular evolution.
1291 Trends Biochem Sci 31, 359–365.
- 1292 McDowall, K.J., Kaberdin, V.R., Wu, S.W., Cohen, S.N., Lin-Chao, S., 1995.
1293 Site-specific RNase E cleavage of oligonucleotides and inhibition by stem-loops.
1294 Nature 374, 287.
- 1295 McDowall, K.J., Lin-Chao, S., Cohen, S.N., 1994. A+U content rather than a
1296 particular nucleotide order determines the specificity of RNase E cleavage. J
1297 Biol Chem 269, 10790–10796.
- 1298 Mehra, A., Hatzimanikatis, V., 2006. An algorithmic framework for genome-wide
1299 modeling and analysis of translation networks. Biophys J 90, 1136–1146.
- 1300 Moffitt, J.R., Pandey, S., Boettiger, A.N., Wang, S., Zhuang, X., 2016. Spatial
1301 organization shapes the turnover of a bacterial transcriptome. Elife 5, e13065.
- 1302 Mohanty, B.K., Kushner, S.R., 2016. Regulation of mRNA decay in bacteria. Ann
1303 Rev Microbiol 70, 25–44.
- 1304 Morozova, N., Zinovyev, A., Nonne, N., Pritchard, L.L., Gorban, A.N., Harel-
1305 Bellan, A., 2012. Kinetic signatures of microRNA modes of action. RNA 18,
1306 1635–1655.
- 1307 Nouaille, S., Mondeil, S., Finoux, A.L., Moulis, C., Girbal, L., Coccagn-Bousquet,
1308 M., 2017. The stability of an mRNA is influenced by its concentration: a
1309 potential physical mechanism to regulate gene expression. Nucleic Acids Res
1310 45, 11711–11724.
- 1311 Pedersen, M.G., Bersanib, A.M., Bersanic, E., 2007. The total quasi-steady-state
1312 approximation for fully competitive enzyme reactions. Bull Math Biol 69, 433.
- 1313 Potts, A.H., Vakulskas, C.A., Pannuri, A., Yakhnin, H., Babitzke, P., Romeo, T.,
1314 2017. Global role of the bacterial post-transcriptional regulator csra revealed
1315 by integrated transcriptomics. Nature Comm 8, 1596.
- 1316 Richards, J., Belasco, J.G., 2019. Obstacles to scanning by RNase E govern bac-
1317 terial mRNA lifetimes by hindering access to distal cleavage sites. Mol Cell 74,
1318 284–295.
- 1319 Richards, J., Luciano, D.J., Belasco, J.G., 2012. Influence of translation on RppH-
1320 dependent mRNA degradation in *Escherichia coli*. Mol Microbiol 86, 1063–1072.

- 1321 Santiago-Frangos, A., Woodson, S.A., 2018. Hfq chaperone brings speed dating to
1322 bacterial sRNA. *RNA* 9, e1475.
- 1323 Schneider, R., Travers, A., Kutateladze, T., Muskhelishvili, G., 1999. A DNA ar-
1324 chitectural protein couples cellular physiology and DNA topology in *Escherichia*
1325 *coli*. *Mol. Microbiol.* 34, 953–64.
- 1326 Schnell, S., Maini, P., 2000. Enzyme kinetics at high enzyme concentration. *Bull*
1327 *Math Biol* 62, 483–499.
- 1328 Segel, L.A., Slemrod, M., 1989. The quasi-steady-state assumption: a case study
1329 in perturbation. *SIAM rev* 31, 446–477.
- 1330 Shalem, O., Groisman, B., Choder, M., Dahan, O., Pilpel, Y., 2011. Transcrip-
1331 tome kinetics is governed by a genome-wide coupling of mRNA production and
1332 degradation: a role for RNA Pol II. *PLoS Genet* 7.
- 1333 Sols, A., Marco, R., 1970. Concentrations of metabolites and binding sites. implica-
1334 tions in metabolic regulation, in: *Curr Topics Cellular Reg.* Elsevier. volume 2,
1335 pp. 227–273.
- 1336 Sousa, S., Marchand, I., Dreyfus, M., 2001. Autoregulation allows *Escherichia*
1337 *coli* RNase E to adjust continuously its synthesis to that of its substrates. *Mol*
1338 *Microbiol* 42, 867–878.
- 1339 Stead, M.B., Marshburn, S., Mohanty, B.K., Mitra, J., Castillo, L.P., Ray, D.,
1340 Van Bakel, H., Hughes, T.R., Kushner, S.R., 2010. Analysis of *Escherichia coli*
1341 RNase E and RNase III activity *in vivo* using tiling microarrays. *Nucleic Acids*
1342 *Res* 39, 3188–3203.
- 1343 Strahl, H., Turlan, C., Khalid, S., Bond, P.J., Kebalo, J.M., Peyron, P., Poljak,
1344 L., Bouvier, M., Hamoen, L., Luisi, B.F., et al., 2015. Membrane recognition
1345 and dynamics of the RNA degradosome. *PLoS Genet* 11, e1004961.
- 1346 Sun, M., Schwalb, B., Schulz, D., Pirkl, N., Etzold, S., Larivière, L., Maier, K.C.,
1347 Seizl, M., Tresch, A., Cramer, P., 2012. Comparative dynamic transcriptome
1348 analysis (cDTA) reveals mutual feedback between mRNA synthesis and degra-
1349 dation. *Genome res* 22, 1350–1359.
- 1350 Suzuki, K., Babitzke, P., Kushner, S.R., Romeo, T., 2006. Identification of a novel
1351 regulatory protein (CsrD) that targets the global regulatory RNAs CsrB and
1352 CsrC for degradation by RNase E. *Genes & Dev* 20, 2605–2617.

- 1353 Tadmor, A., Tlusty, T., 2008. A coarse-grained biophysical model of *E. coli* and
1354 its application to perturbation of the rRNA operon copy number. PLoS Comput
1355 Biol 4, e1000038–e1000038.
- 1356 Tang, J., Riley, W., 2013. A total quasi-steady-state formulation of substrate
1357 uptake kinetics in complex networks and an example application to microbial
1358 litter decomposition. Biogeosciences 10, 8329–8351.
- 1359 Tang, J., Riley, W., 2017. SUPECA kinetics for scaling redox reactions in networks
1360 of mixed substrates and consumers and an example application to aerobic soil
1361 respiration. Geosci Model Dev 10, 3277–3295.
- 1362 Thomas, P., Terradot, G., Danos, V., Weiße, A.Y., 2018. Sources, propagation
1363 and consequences of stochasticity in cellular growth. Nat Commun 9, 4528.
- 1364 Tzafiriri, A., 2003. Michaelis-Menten kinetics at high enzyme concentrations. Bull
1365 Math Biol 65, 1111–1129.
- 1366 Tzafiriri, A., Bercovier, M., Parnas, H., 2002. Reaction diffusion model of the
1367 enzymatic erosion of insoluble fibrillar matrices. Biophys J 83, 776–793.
- 1368 Tzafiriri, A., Edelman, E., 2004. The total quasi-steady-state approximation is
1369 valid for reversible enzyme kinetics. J Theor Biol 226, 303 – 313.
- 1370 Valgepea, K., Adamberg, K., Seiman, A., Vilu, R., 2013. *Escherichia coli* achieves
1371 faster growth by increasing catalytic and translation rates of proteins. Mol
1372 Biosyst 9, 2344–2358.
- 1373 Wang, Y., Liu, C.L., Storey, J.D., Tibshirani, R.J., Herschlag, D., Brown, P.O.,
1374 2002. Precision and functional specificity in mRNA decay. Proc Natl Acad Sci
1375 USA 99, 5860–5865.
- 1376 Weiße, A.Y., Oyarzún, D.A., Danos, V., Swain, P.S., 2015. Mechanistic links
1377 between cellular trade-offs, gene expression, and growth. Proc Natl Acad Sci
1378 USA 112, E1038–E1047.
- 1379 Wright, P.R., Georg, J., Mann, M., Sorescu, D.A., Richter, A.S., Lott, S.,
1380 Kleinkauf, R., Hess, W.R., Backofen, R., 2014. CopraRNA and IntaRNA: pre-
1381 dicting small RNA targets, networks and interaction domains. Nucleic Acids
1382 Res 42, W119–W123.
- 1383 Yandek, L.E., Lin, H.C., Harris, M.E., 2013. Alternative substrate kinetics of *Es-*
1384 *cherichia coli* ribonuclease P determination of relative rate constants by internal
1385 competition. J Biol Chem 288, 8342–8354.